Quaternary Science Reviews 169 (2017) 13–28

Contents lists available at ScienceDirect

Quaternary Science Reviews

journal homepage: www.elsevier.com/locate/quascirev

Invited review

Current state and future perspectives on coupled ice-sheet – sea-level modelling

Bas de Boer [a, b, *], Paolo Stocchi [c], Pippa L. Whitehouse [d], Roderik S.W. van de Wal [a]

[a] Institute for Marine and Atmospheric Research Utrecht, Utrecht University, PO BOX 80.005, 3508 TA Utrecht, The Netherlands
[b] School of Earth and Environment, University of Leeds, Woodhouse Lane, Leeds, LS2 9JT, United Kingdom
[c] NIOZ Royal Netherlands Institute for Sea Research, PO Box 59, 1790 AB, Den Burg, Texel, The Netherlands
[d] Department of Geography, Durham University, Lower Mountjoy, South Road, Durham, DH1 3LE, United Kingdom

ARTICLE INFO

Article history:
Received 25 November 2016
Received in revised form
28 April 2017
Accepted 12 May 2017
Available online 29 May 2017

Keywords:
Quaternary
Ice sheet model
Sea level changes
Global
Glacial isostatic adjustment
Self-gravitation
Coupling

ABSTRACT

The interaction between ice-sheet growth and retreat and sea-level change has been an established field of research for many years. However, recent advances in numerical modelling have shed new light on the precise interaction of marine ice sheets with the change in near-field sea level, and the related stability of the grounding line position. Studies using fully coupled ice-sheet – sea-level models have shown that accounting for gravitationally self-consistent sea-level change will act to slow down the retreat and advance of marine ice-sheet grounding lines. Moreover, by simultaneously solving the 'sea-level equation' and modelling ice-sheet flow, coupled models provide a global field of relative sea-level change that is consistent with dynamic changes in ice-sheet extent. In this paper we present an overview of recent advances, possible caveats, methodologies and challenges involved in coupled ice-sheet – sea-level modelling. We conclude by presenting a first-order comparison between a suite of relative sea-level data and output from a coupled ice-sheet – sea-level model.

1. Introduction

Global sea-level records, particularly those dating from the Quaternary glacial cycles, provide crucial insight into past ice-sheet change. Interpreting the complex relationship between spatially-variable sea-level change and the growth and decay of the major ice sheets forms the basis of the field of Glacial Isostatic Adjustment (GIA). Traditionally, GIA models have been used to understand the impact of ice-sheet change on global sea level. This study describes recent efforts to understand feedbacks in the opposite direction, namely, the impact of spatially-variable sea-level change on ice-sheet dynamics. Theories relating to the gravitational attraction between the ice sheets and the ocean were first proposed in the late 19th century (e.g. Woodward, 1888, and reference therein), but it was only in the 1970s that gravitational effects began to be accounted for in calculations of global sea-level. Woodward (1888) had demonstrated that the gravitational potential at the outer surface of the Earth would be perturbed due to a change in mass at a point. However, in order to accurately determine the details of the perturbation, and hence calculate how meltwater would be distributed across the ocean, this also required the establishment of viscoelastic Green functions for the radial displacement of the solid Earth (Peltier, 1974) and the perturbation of the gravitational potential (Peltier and Andrews, 1976). This theory was then applied to the problem of global sea-level change by Farrell and Clark (1976), who additionally accounted for mass conservation during the transition from continental loading by ice sheets to meltwater redistribution throughout the ocean.

These studies from the 1970s provided the first statement of the sea-level equation (SLE), which forms the basis of all contemporary GIA models, and accounts for the gravitational attraction of ice sheets on the ocean, as well as the deformation of the Earth due to changes in ice loading and the redistribution of ocean water. From the 1980s to the early 2000s a number of improvements were made to the theory originally laid out by Clark et al. (1978), with the result that GIA models now typically also account for rotational feedback effects and shoreline migration, as well as the inundation of ocean water into regions previously

* Corresponding author. Institute for Marine and Atmospheric Research Utrecht, Utrecht University, PO BOX 80.005, 3508 TA Utrecht, The Netherlands.
E-mail address: b.deboer@uu.nl (B. de Boer).

http://dx.doi.org/10.1016/j.quascirev.2017.05.013

covered by marine-grounded ice (e.g. Wu and Peltier, 1984; Peltier, 1994; Kendall et al., 2005).

The SLE is typically solved using the 'pseudo-spectral' approach (e.g. Mitrovica and Peltier, 1991; Mitrovica et al., 1994) for a 1-D spherically symmetric Earth. Calculations are carried out using a particular maximum spherical harmonic degree (e.g. 128, 256 or 512), which defines the spatial resolution of the solution to the SLE. After iteratively solving the SLE, the solution is given by:

$$\Delta S = \Delta N - \Delta U. \quad (1)$$

Here ΔS is relative sea-level (RSL) change, given as the difference between the change in sea-surface height, ΔN, and the deformation of the Earth ΔU. The shape of the sea surface is defined by the shape of the gravitational equipotential surface, or geoid. The deformation of the Earth is usually determined by considering a radially-symmetric Earth model. In addition to defining an Earth model, the history of global ice loading must also be prescribed in order to solve the SLE. Most well-known and widely-used within the field of GIA are the ICE-NG global ice-sheet reconstructions, e.g. ICE-3G (Tushingham and Peltier, 1992), ICE-5G (Peltier, 2004) and more recently ICE-6G_C (Peltier et al., 2015). These global reconstructions were derived via the comparison of GIA model output with a global suite of field data, including RSL data.

A similar data-driven approach has been used to constrain or tune regional ice-sheet reconstructions, e.g. for Fennoscandia (Lambeck et al., 1998), the British Isles (Bradley et al., 2011), Arctic Canada (Simon et al., 2015) and Antarctica (Ivins and James, 2005; Ivins et al., 2013), while some studies have additionally made use of a numerical (3-D) ice-sheet model to determine glaciologically-consistent, climatically-forced changes to the Greenland (Tarasov and Peltier, 2002; Simpson et al., 2009; Lecavalier et al., 2014), North American (Tarasov and Peltier, 2004; Tarasov et al., 2012) and Antarctic (Whitehouse et al., 2012a, b; Briggs et al., 2013) ice sheets.

Solutions to the SLE describe the gravitationally self-consistent change in RSL that would arise due to forcing by the prescribed ice-sheet history. Fig. 1 illustrates in a schematic way how a change in ice-sheet volume will affect RSL. In the absence of self-gravitational effects and solid Earth deformation, a change in ice-sheet volume would result in a uniform change in sea level (Fig. 1b). However, including self-gravitation and solid Earth deformation means that the change in RSL over the globe is non-uniform. For a decrease in ice volume, RSL will fall close to the ice sheet but rise by an amount greater than the global mean at far-field sites (Fig. 1c). As an example, when the ice-sheet is described as a point source, a fall in RSL will be seen up to $\sim$ 2200 km from the ice sheet, and a rise by an amount greater than the mean will be seen at sites more than $\sim$ 6700 km from the ice sheet (e.g. Vermeersen and Sabadini, 1999). This spatial variability in the sea-level response can be used to infer the pattern of past ice-sheet change (e.g. Clark et al., 1978; Peltier, 2004).

Alongside studies that use sea-level records to determine past ice sheet change, the ice-sheet modelling community has also sought to reconstruct changes in global ice volume. Early studies used vertically-averaged models (Oerlemans, 1982; Pollard, 1982), but since the 1990s more sophisticated models have been used to reconstruct changes to specific ice sheets (e.g. Huybrechts, 1990; Deblonde et al., 1992; Ritz et al., 1997; Tarasov and Peltier, 1999; Van de Wal, 1999; Huybrechts, 2002; Tarasov and Peltier, 2003; DeConto and Pollard, 2003; Zweck and Huybrechts, 2005; Philippon et al., 2006; Pollard and DeConto, 2009; Bintanja and Van de Wal, 2008; De Boer et al., 2013; Stuhne and Peltier, 2015). All models referred to above use an approximation of the full Stokes equation of ice flow. Most notably, the shallow ice approximation

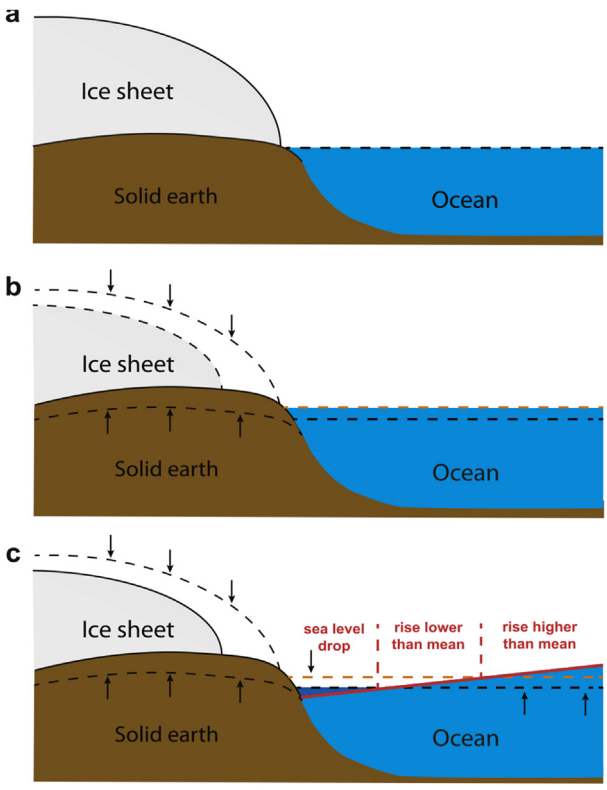

Fig. 1. A schematic representation of the gravitational interaction between ice sheets, the solid Earth and the ocean. a) The initial state of the system: For illustrative purposes we take the initial sea surface to be horizontal. b) A decrease in ice-sheet mass will result in rebound of the solid Earth beneath the ice sheet and an increase in ocean volume. In (b) we show the change in sea level as uniform, but in reality due to self-gravitation effects the sea surface will fall in close proximity to the ice sheet, it will rise by an amount less than the mean at mid-field locations, and it will rise by an amount greater than the mean at far-field locations. The initial sea surface from panel (a) is illustrated in (b) and (c) by the horizontal dashed black line. The horizontal dashed orange line in (b) and (c) represents the sea surface following ice mass loss in the absence of self-gravitation from panel (b). The dark blue area indicates the region of sea-level fall, and the solid red line represents the actual sea surface.

(SIA), which only considers shear stresses, is assumed to govern the flow of grounded ice (Hutter, 1983), while the shallow shelf approximation (SSA), which only considers longitudinal stresses, is assumed to govern the flow of floating ice shelves (Morland, 1987). Although these approximations reduce the computational cost of running an ice-sheet model for long-term paleoclimate simulations, it has been shown that more sophisticated physics are needed to accurately represent grounding-line migration (e.g. Bueler and Brown, 2009; Larour et al., 2012; Cornford et al., 2013), or to reproduce observed lateral gradients in ice velocity (Rignot et al., 2011).

In recent years several studies have emerged that include additional physical mechanisms aimed at improving model representations of grounding-line migration (e.g. Schoof, 2007; Bueler and Brown, 2009; Gladstone et al., 2010; Pollard and DeConto, 2012; Seroussi et al., 2014; Feldmann et al., 2014). When comparing output from these models it is clear that results may diverge significantly for different grounding-line approximations, levels of model complexity, or horizontal resolution (Pattyn et al., 2013; Bindschadler et al., 2013; Pattyn and Durand, 2013; Feldmann et al., 2014). However, so far, uncertainty associated with the grounding-line response to sea-level forcing has not been quantified. Ice flux across the grounding line is strongly dependent

on water depth, i.e. the RSL, at the grounding line (Schoof, 2007), and model behaviour may therefore differ, depending on how this forcing is parametrised.

In this review we discuss a relatively new area of research, in which changes in ice volume depend on gravitationally self-consistent, spatially-variable changes in RSL at the ice sheet grounding line. These self-consistent ice-sheet and sea-level reconstructions can be produced by coupling a GIA model to an ice-sheet model (e.g. Gomez et al., 2012, 2013; De Boer et al., 2014; Konrad et al., 2014), and they reflect an integrated approach to understanding sea-level change over glacial-interglacial cycles. In Section 2 we present an overview of recent advances in coupled ice-sheet – sea-level modelling and describe a number of features that should be included in the near future. The main advantages of these coupled models are that: (i) the effects of non-eustatic RSL change on marine ice-sheet stability can be more realistically represented; and (ii) ice sheet and sea-level changes are internally consistent, permitting a more robust comparison of model output with global RSL data.

Most ice-sheet models are run assuming that the accompanying sea-level change is uniform (e.g. De Boer et al., 2013), or they are forced using an estimate of past global mean sea-level change (e.g. Huybrechts, 2002). However, GIA modelling clearly indicates that RSL changes at the grounding line will strongly deviate from the global mean. Accounting for self-gravitational effects within a coupled ice-sheet – sea-level model allows for more realistic sea-level forcing to be applied at the ice-sheet grounding line.

The stability of a marine-grounded ice sheet is strongly dependent on the gradient of the bed. Marine ice sheets lying on a retrograde sloping bed are hypothesised to be unstable and susceptible to rapid grounding-line retreat due to the increase in ice thickness upstream (Weertman, 1974). This instability has been shown to depend on basal properties of the bed, accumulation rates and ocean forcing (e.g. Schoof, 2007; Pattyn et al., 2012; Robel et al., 2016). In order to accurately determine the past and present stability of marine-grounded ice sheets such as Antarctica, it is also important to include realistic sea-level forcing in future studies as it has already been shown to have a stabilising effect on marine ice-sheet dynamics (Gomez et al., 2010). When considering the factors contributing to this process, one should note that as the grounding line retreats, marine-grounded ice at flotation will be immediately replaced by an equivalent mass of ocean water. Hence, the instantaneous net change in surface loading right at the grounding line will be negligible. However, grounding line retreat is invariably driven by regional ice loss; it is this regional decrease in ice mass that triggers solid Earth rebound and a local drop in the height of the geoid, with the net effect being a decrease in water depth at the grounding line.

A suite of data, including RSL data, ice-extent data, and present-day uplift rates based on GPS measurements, are now available for a direct comparison with a coupled ice-sheet – sea-level model (e.g. Briggs et al., 2014; Argus et al., 2014; Peltier et al., 2015; Hughes et al., 2016). In Sections 3 and 4 we focus on a comparison with RSL data during the late Quaternary to determine the accuracy of a recent global ice-sheet reconstruction that has been derived using a coupled ice-sheet – sea-level model.

2. Current state and recent advances in coupled ice-sheet – sea-level models

A coupled model of dynamic ice-sheet change and gravitationally self-consistent sea-level change is schematically illustrated in Fig. 2. The ice-sheet model determines the change in ice-sheet thickness through time, which in turn determines the change in global mean sea level (eustasy) and surface loading by ice. This

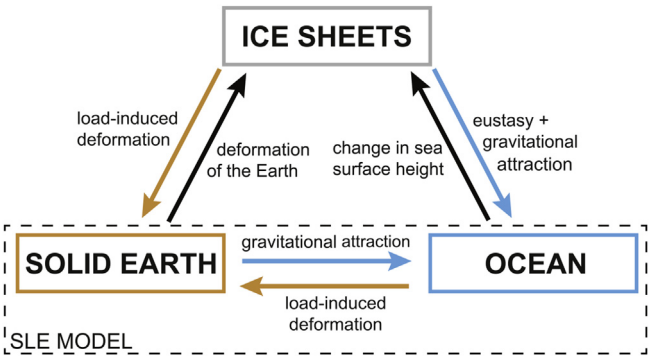

Fig. 2. Diagram of the coupled systems discussed here, describing the interactions between ice sheets, the solid Earth and the ocean. Ice sheets are modelled with an ice-sheet model, the response of the solid Earth is calculated using a viscoelastic Earth model, and changes to the ocean (sea surface) reflect changes in the shape of the geoid. Together, the solid Earth and ocean components represent the change in RSL as determined by solving the SLE (dashed box).

information is fed into the SLE solver, which simultaneously solves for the deformation of the Earth and consequent changes to the shape of the sea surface. This calculation must be carried out iteratively because the re-distribution of ocean water as well as ice mass will deform the solid Earth (see Section 2.1). The combined effects of changes to the height of the solid Earth and the sea surface (black arrows in Fig. 2) results in the change in RSL. Changes in water depth, i.e. RSL, are important for ice-sheet advance and retreat and are fed back into the ice-sheet model every coupling time step.

As has already been shown (Gomez et al., 2013; De Boer et al., 2014), coupled simulations of 3-D ice-sheet and sea-level change predict different behaviour for the advance and retreat of the West Antarctic ice sheet (WAIS) during the last glacial cycle compared with non-coupled simulations (Fig. 3). In particular, the predicted increase in the volume of the WAIS during the last glacial cycle is smaller in the coupled simulations due to negative feedbacks associated with an increase in near-field water depth driven by the deformation of the solid Earth and the gravitational attraction of the growing ice sheet. Similarly, ice-sheet retreat is delayed in the coupled simulations due to the counter-intuitive fall in near-field RSL resolved by the coupled model; this is in stark contrast with the increase in RSL prescribed by traditional global mean sea-level forcing (Gomez et al., 2013; De Boer et al., 2014). Gomez et al. (2013) found that the limited Antarctic RSL data set could not robustly discriminate between the coupled and uncoupled simulations. However, they found that GPS observations of uplift rates did show an improved fit for the coupled simulations.

The studies shown in Fig. 3 represent just two model realisations of Antarctic ice volume change during the last glacial cycle. These models differ, both from each other and from other simulations of Antarctica during the Last Glacial Maximum (LGM) (e.g. Whitehouse et al., 2012a; Golledge et al., 2013; Briggs et al., 2014; Maris et al., 2014; Stuhne and Peltier, 2015), reflecting that it is still largely unresolved how to most accurately simulate the past evolution of the Antarctic Ice Sheet (AIS). Uncertainties are quantified in these papers by either: changing the ocean or sea-level forcing (Golledge et al., 2013), changing model parameters (Whitehouse et al., 2012a; Maris et al., 2014), or evaluating a large ensemble of model runs (Briggs et al., 2014). In the recent paper of Stuhne and Peltier (2015) data assimilation methods are used to seek the optimum fit to the observational constraints, but the authors note that non-uniqueness still exists, in part due to error bars on these observational constraints.

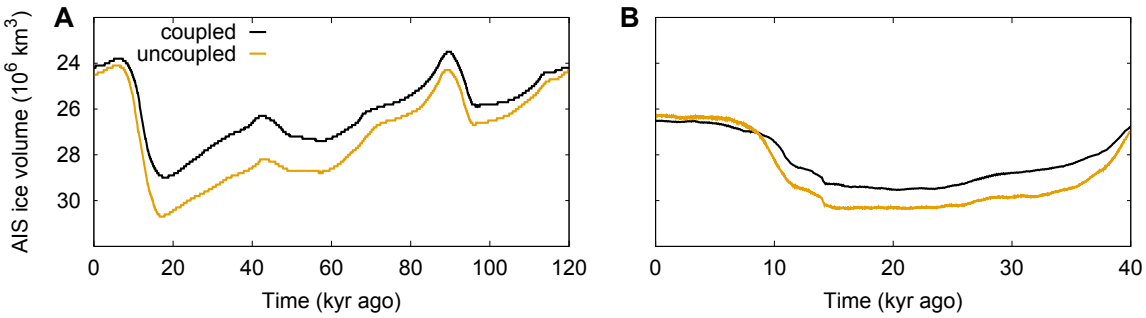

Fig. 3. Simulated ice volume on land (in 10^6 km^3) of the Antarctic ice sheet. The coupled ice-sheet sea-level simulations are shown in black, the uncoupled simulations that are driven by global mean sea level are shown in orange. a) Simulations as presented in De Boer et al. (2014) shown here from 120 kyr ago to present, b) simulations as presented in Gomez et al. (2013) from 40 kyr ago to present.

Accounting for feedbacks between ice dynamics and GIA will also be very important when considering the future evolution of the predominantly marine-grounded WAIS. As described in the review of Joughin and Alley (2011), the WAIS is susceptible to unstable retreat due to its contact with the ocean. It is currently buttressed by large floating ice shelves, and in a warming climate these ice shelves are predicted to lose mass, either by the calving of icebergs or through basal melting following contact with warm ocean water (Depoorter et al., 2013). A decrease in the extent or thickness of the ice shelves will reduce the magnitude of buttressing applied to those parts of the WAIS that are grounded below sea level, this can trigger an increase in ice flux, and it may lead to unstable grounding line retreat in areas where the bed deepens upstream (Weertman, 1974). However, most studies that predict unstable ice mass loss do not consider GIA feedbacks, despite the fact that they have been shown to have a stabilising effect on grounding line retreat, even on an upstream-deepening bed (Gomez et al., 2010).

Accounting for gravitationally self-consistent sea-level change will also be important when studying the evolution of other marine-based ice sheets. Parts of East Antarctica, in particular the Wilkes, Aurora and Recovery basins, are grounded below sea level (Fretwell et al., 2013). The ice sheet will therefore be sensitive to near-field sea-level change in these regions, particularly if the buttressing ice shelves disappear under warmer-than-present climate scenarios (e.g. Pollard et al., 2015). The Eurasian and North American ice sheets that have waxed and waned during the Quaternary largely terminated on land. However, during their maximum extent both ice sheets will have been in contact with the ocean and/or shallow seas and thus will have been susceptible to local RSL change (e.g. Kleman et al., 2013; Ingólfsson and Landvik, 2013). As an example, in Fig. 4 we illustrate the differences in Eurasian and Antarctic ice thickness 20.000 years (20 kyr) after the start of a Quaternary glacial cycle that can be attributed to the use of either a coupled ice-sheet – sea-level model or an uncoupled ice-sheet model. Both models account for the visco-elastic solid Earth response to ice-load change but the uncoupled model is driven by global mean sea-level change, whereas the coupled model is driven by spatially-varying RSL change. Both ice sheets are predicted to be thinner across the marine-based regions of the Barents Sea and West Antarctica when coupling is taken into account (De Boer et al., 2014).

The results presented in Figs. 3 and 4 demonstrate the importance of using a coupled ice-sheet – sea-level model to understand the behaviour of a marine-based ice sheet. In the following subsections we discuss a number of important factors that must be taken into consideration when building a coupled ice-sheet – sea-level model.

2.1. Forward modelling of RSL change

Solving the SLE allows us to determine how RSL changes through time and how such changes play an important role in governing ice-sheet dynamics. In an uncoupled GIA model, where the ice history is pre-defined, a simple way to proceed is to (i) calculate the solid Earth response to ice and ocean load change across a given time interval assuming that melt water is distributed uniformly across the ocean, (ii) calculate the change to the shape of the geoid due to the redistribution of mass (ice, ocean and solid Earth) across this time interval, and (iii) consequently determine how the melt water will really be distributed across the ocean. However, there is a complication here, because a spatially-variable change in ocean loading will deform the Earth differently to a uniform change in ocean loading, this impacts on the shape of the geoid, and hence the distribution of melt water. Therefore, the SLE must be solved iteratively, hereby also accounting for rotational feedback effects, shoreline migration and the inundation of ocean water into regions previously covered by marine-grounded ice. Typically, a GIA model is run several times, forced by the full pre-defined ice-sheet history, until the solution for RSL change through time converges (e.g. Peltier, 1998; Kendall et al., 2005; Spada and Stocchi, 2007).

This solution for RSL change through time can be used to calculate absolute changes in water depth during the GIA model run as given by equation (1). Although, once again, this is an iterative process for which some initial distribution of water depth at the start of the model run must first be assumed. The incremental changes in RSL output by the GIA model can then be used to determine the evolution of water depth as the model is integrated forward in time. However, this does not guarantee that the modelled water depths over the globe will match present-day observed water depths at the end of the model run. To ensure that the final topography at the end of the simulation matches the observed topography at present day, the misfit between modelled and observed present-day water depths could be applied as a correction to the initial topography. This process should be repeated, and the full simulation re-run, until convergence is met (e.g. Kendall et al., 2005; Gomez et al., 2013).

Unfortunately, it is not possible to robustly calculate absolute water depth change with time unless the GIA model has been run all the way through to the present day, i.e. if we know how past incremental changes in RSL relate to present-day water depths. For example, a GIA model could be used to calculate the change in RSL between 20 and 10 kyr ago, but without knowing how RSL changed between 10 kyr ago and the present it is not possible to relate the changes between 20 and 10 kyr ago to absolute water depths.

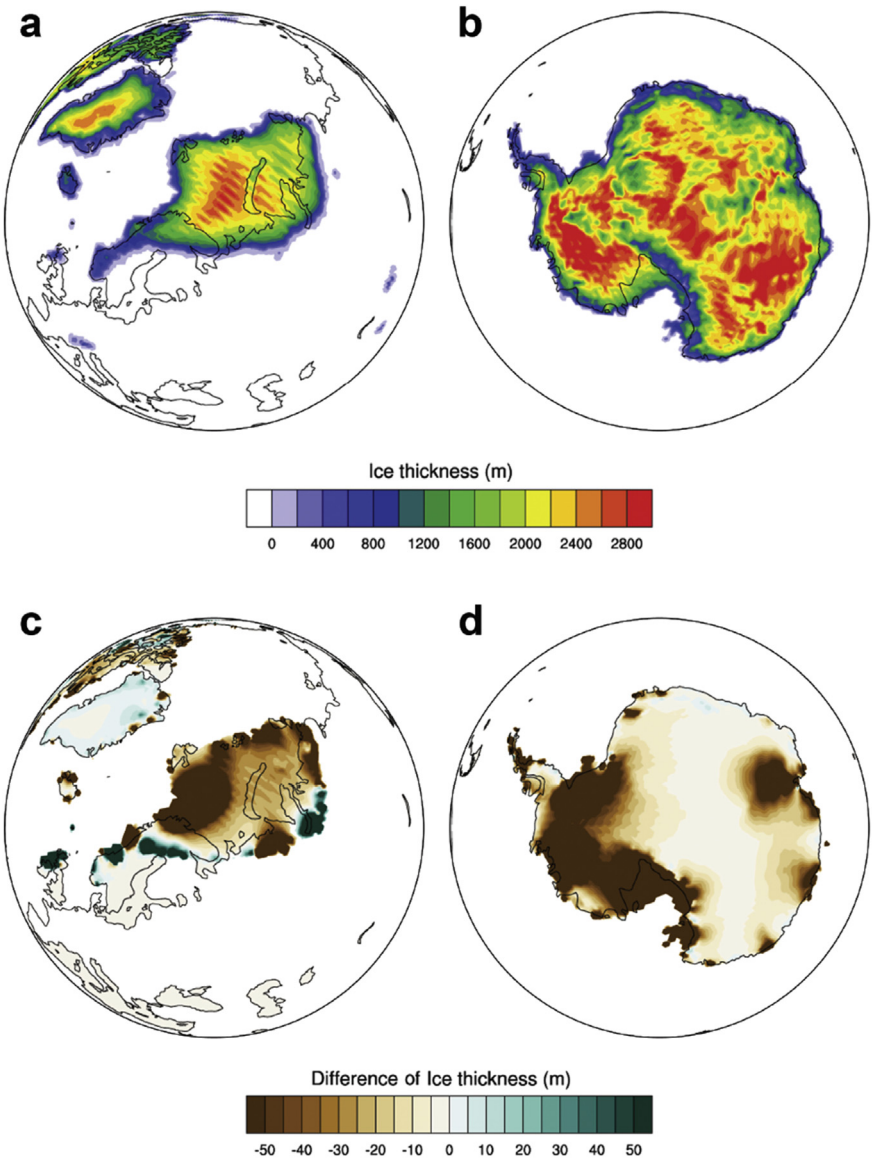

Fig. 4. Simulated ice sheets from the runs in De Boer et al. (2014) at 380 kyr ago, about 20 kyr into the first glacial cycle of the experiment. Ice thickness across a) Eurasia and b) Antarctica as simulated with the coupled ice-sheet – sea-level model. Difference in ice thickness across c) Eurasia and d) Antarctica between the coupled and uncoupled simulations. Both models use the same viscoelastic Earth model, but the uncoupled model is driven by global mean sea-level change, whereas the coupled model is driven by spatially-varying RSL change.

Crucially, absolute water depth is the variable that feeds into the ice-sheet model.

It is clear from the previous two paragraphs that it is non-trivial to determine absolute water depth at some time in the past without knowing the full ice-sheet history, due to the necessity of relating past changes to present water depths. However, the ice-sheet history is simulated incrementally forwards in time, to take account of inherent feedbacks and lags in the system, e.g. associated with the viscoelastic nature of the mantle. This poses a problem when running a coupled ice-sheet – sea-level model. Gomez et al. (2013) address this issue by using an initial guess for the topography and ice-sheet configuration of the AIS 40 kyr ago, as output from a long Plio-Pleistocene simulation (Pollard and DeConto, 2009), while the ice sheets outside of the AIS are prescribed using the ICE-5G models (Peltier, 2004). After running the coupled model for 40 kyr the initial global topography is adjusted using the misfit to present, and the process is repeated until convergence for the present-day topography is met.

A different approach is taken by De Boer et al. (2014) who coupled four ice-sheet models, representing ice volume over North America, Eurasia, Greenland and Antarctica, to a GIA model and ran simulations over multiple glacial cycles. This procedure is too time consuming to iterate over all previous time steps to reach convergence. Two factors made their task feasible. First, they assumed that topography and water depths at the start of their model run were the same as present. This allowed them to estimate absolute water depths as the model ran forwards through time, and it meant that the coupled model only had to be run once. It does, however, mean that convergence is not achieved for the present-day solution, and hence for a comparison with RSL data, model output needs to be corrected for the mismatch to present-day water depth. Second, past changes in RSL, including the elastic and viscous response of

the Earth, were saved in a temporary array that extends sufficiently far back in time for the SLE to be solved at each GIA model time step (see De Boer et al., 2014, for details). This array was reloaded every time information was passed between the ice-sheet model and the sea-level model, and it was updated with the RSL change for the most recent time step. The advantage of this method is that ongoing changes to the shape of the solid Earth and the geoid - which arise due to past changes in RSL - are taken into account when calculating RSL change at the most recent time step. The coupling time step used by De Boer et al. (2014) was 1000 years, whereas Gomez et al. (2013) used a time step of 200 years. Both studies carried out tests where the coupling time step was reduced by up to a factor of ~ 4, but the results did not change significantly.

2.2. Calculating variations in ocean area and grounding line position

The mean change in RSL across each time step of a GIA model will depend on (i) the change in global ice volume, and (ii) the contemporaneous area of the ocean. Changes in ocean area due to the migration of terrestrial coastlines have been considered within GIA models for many years (e.g. Johnston, 1993; Peltier, 1994; Milne and Mitrovica, 1996; Milne et al., 1999; Mitrovica and Milne, 2003; Kendall et al., 2005). At each time step, palaeo-topography (the negative of absolute water depth) is used to determine a temporally-varying ocean mask, which is then used to calculate the mean change in RSL across that time step. Absolute palaeo-topography values can only be calculated after the GIA model has been run through to the present day, and they may vary between iterative solutions to the SLE. Consequently, the time-varying shape of the ocean mask may vary between model iterations.

Similarly, changes in ocean area due to changes in the areal extent of ice sheets have also gradually been implemented within GIA models (e.g. Peltier, 1994; Milne and Mitrovica, 1998; Kendall et al., 2005). In an uncoupled model, evolution of the ocean mask in the region of a marine-grounded ice sheet is largely pre-defined by the assumed ice history, although if a flotation criterion is used to check whether ice is floating or grounded, the ocean mask can change between iterations of the SLE due to changes to the solution for RSL. In a coupled model, the position of the grounding line is free to evolve, and hence the evolution of the ocean mask will be an output of the model (e.g. see Fig. 8f in De Boer et al., 2014). As alluded to above, if the ice-sheet model includes a representation of ice shelves, a flotation test must be used to correctly identify the position of the grounding line at each time step of the GIA model (bearing in mind that the GIA model and the ice-sheet model will likely be run at different spatial resolutions; see next section):

$$\frac{\rho_i}{\rho_w} H_i > S. \tag{2}$$

Here, H_i is ice thickness, ρ_i and ρ_w are the density of ice and sea water respectively, and S is the local water depth, which is positive where the bed is below sea level. In regions where this inequality holds, i.e. upstream of the grounding line, surface load changes are prescribed by changes in ice thickness. In regions where H_i is positive but this inequality does not hold, i.e. downstream of the grounding line, surface load changes are solved for within the GIA model assuming this region is filled with ocean water that follows the shape of the geoid. This assumption holds since any floating ice shelves will approximately be in hydrostatic equilibrium.

When an ice sheet shrinks and the grounding line retreats (Fig. 5a to b), this leads to a decrease in the gravitational attraction of the ice sheet due to the decrease in its mass. This in turn leads to a decrease in local RSL, which can trigger grounding-line advance

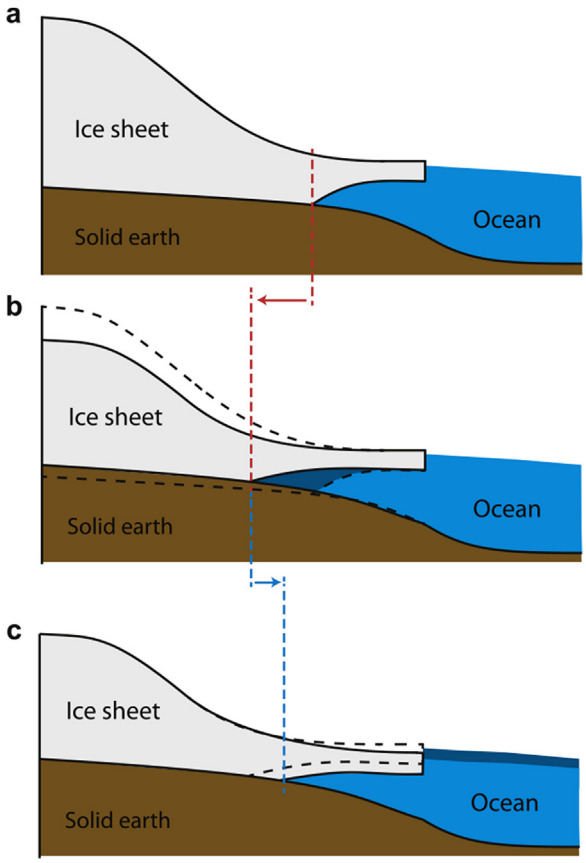

Fig. 5. A schematic representation of the migration of the coastline near ice sheets. a) the initial state of the ice-sheet-shelf system. The grounding line, and thus the coastline, is illustrated by the red dashed line. b) The retreated ice sheet at the next time step, the previous ice-sheet topography (panel a) is given by the black dashed lines. The elastic response of the bedrock is shown. The new grounding line is indicated by the red dashed line. c) After solving the SLE, the near field RSL has dropped due to a decrease in the gravitational attraction of the smaller ice sheet. The final grounding line is illustrated by the blue dashed line.

(Fig. 5b to c). To understand the reason for this response, note that ice flux across the grounding line has been shown to be strongly dependent on the thickness of ice at the grounding line (Schoof, 2007), and hence the water depth S (equation (2)). If the local water depth (RSL) decreases this will lead to a decrease in ice flux across the grounding line. Assuming no change in mass input, i.e. accumulation, a sufficient decrease in ice flux (mass output) will return the ice sheet to a situation of positive mass balance, leading to ice thickening and grounding line advance. It is especially important to account for GIA-related feedbacks on water depth in regions where the ice sheet thickens upstream, since it has been shown that this can prevent runaway ice loss from an otherwise unstable configuration (Gomez et al., 2010). Whether the grounding line retreats or advances thus depends on the local settings of the slope of the bedrock topography, ice thickness and on the surface or basal mass balance. We conclude this section by noting that being able to account for changes in coastline and grounding-line position thus results in an interplay between ice dynamics and local RSL change in a coupled model (Fig. 5).

2.3. Solving the SLE on the horizontal mesh

As mentioned in Section 2.1, solving the SLE requires a time-consuming iterative procedure. According to the SLE, RSL change

at a specific location and time depends on all previous ice and RSL variations that have occurred at any place on Earth. Therefore, spatio-temporal convolutions over the surface of the Earth and throughout the ice-sheet loading history are necessary. In addition, the requirement that at any place and time the mean sea surface corresponds to an equipotential surface of gravity (geoid), together with the constraint of mass conservation, demands that an iterative procedure must be adopted. The spatio-temporal convolution is repeated at each iterative step until convergence is achieved. Allowing for coastline migrations (and therefore topography changes) as mentioned in Section 2.2 is another reason that the whole procedure must be repeated typically 3 times before convergence is achieved.

To give an example of the horizontal mesh used in a GIA model, we here discuss SELEN as used in De Boer et al. (2014). The horizontal mesh that is used in SELEN is computed using icosahedral pixelisation (Tegmark, 1996) and it consists of almost equal-area hexagonal elements that allow for a nearly optimal quadrature on the sphere. The size of the hexagonal elements is defined by the *RES* parameter, which implies a total number of elements given by:

$$N_P = 40 \times RES(RES - 1) + 12. \quad (3)$$

For example, in the simulations presented by De Boer et al. (2014) $RES = 60$, giving a total number of SELEN elements of 141612 and a grid distance of about 48 km. Increasing the resolution of a simulation leads to a higher value of N_P and clearly results in a longer spatio–temporal convolution of the SLE and longer computation time. In the fully coupled ice-sheet – sea-level system a high spatial resolution, on the order of ~ 10 km or less, in the glaciated areas is desirable in order to describe the physics that are related to ice flow, while in coastal regions it is desirable in order to accurately represent the distribution of ocean loading. However, if this high resolution was used everywhere this would result in a significant increase of computational time. The use of a heterogeneous mesh would then be a favourable solution to this issue. For example, Adhikari et al. (2016) used an unstructured mesh to calculate short-timescale variations of RSL change. The mesh model could also improve the coupling of sea level and 3-D ice-sheet models, for example by enhancing the realistic simulation of kilometre-scale outlet glaciers (Adhikari et al., 2016). Later on in Section 6 we will discuss the implementations of a heterogeneous mesh in SELEN.

2.4. Modelling the deformation of the solid Earth

When solving the SLE it is commonly assumed that the Earth is radially stratified, and the mantle has a linear viscoelastic rheology (Spada and Stocchi, 2007). In that case, the Earth is represented by an elastic lithosphere of a certain thickness, commonly on the order of 50–200 km, and a radially stratified 1-D viscoelastic Earth with n layers. The value of n is typically chosen to be 2 or 3 (Dziewonski and Anderson, 1981; Spada et al., 2004), with the viscosity of the upper and lower mantle typically assumed to be on the order of 10^{20} -10^{21} Pa and 10^{21} -10^{23} Pa, respectively (e.g. Peltier, 2004; Spada et al., 2004).

Because of these assumptions, most contemporary ice-sheet – sea-level models do not capture lateral variations in Earth structure. However, a key factor in determining the precise interaction between ice-sheet advance/retreat and the response of the Earth is the Earth's rheology itself, which will vary with location. For example, beneath West Antarctica the lithosphere is generally thinner than the global average, and the mantle viscosity is lower (Morelli and Danesi, 2004; An et al., 2015; Van der Wal et al., 2015), meaning that rebound will take place relatively rapidly in response to ice loss (e.g. Nield et al., 2014). This is taken into account in the coupled-model projections of Gomez et al. (2015) and Konrad et al. (2015), who show that the rebound rates associated with a sufficiently weak Earth model can act to delay or even stabilise the retreat of the AIS under some future climate scenarios.

3. Indicators of relative sea level

One of the main advantages of using a coupled ice-sheet – sea-level model is that it permits a more robust comparison of modelled and observed RSL, both spatially and temporally. Here, we present a small selection of the available RSL data for two different time slices during the late Quaternary, including near and far fields sites. Firstly, we consider the last interglacial, or the Eemian, a period thought to be warmer than present with RSL higher than today, focusing on the retreat towards the Eemian and the glacial inception thereafter, between 135 and 105 kyr ago. Secondly, we consider the last termination, the glacial retreat from the LGM. For this period, we focus on changes across Antarctica between 12 and 0 kyr ago. In Section 4, we present a preliminary comparison of model output with the RSL data described here.

3.1. Last interglacial (Eemian)

The Eemian is the interglacial period before the inception of the last glacial cycle, from ~ 130 to ~ 115 kyr ago. It is generally considered to be a period of global, although nonuniform, warmth relative to the present (CAPE Last Interglacial Project Members, 2006; Capron et al., 2014). During the Eemian, sea level is thought to have been higher than present and also variable over the globe (Thompson and Goldstein, 2005; Lambeck et al., 2006; Rohling et al., 2008; Kopp et al., 2009; Grant et al., 2012; O'Leary et al., 2013; Long et al., 2015), whereas atmospheric carbon dioxide concentrations were similar to pre-industrial levels (Petit et al., 1999) and insolation varied significantly during this time (Laskar et al., 2004). Current estimates for global mean sea-level during this period vary from 6 to 9 m (Dutton et al., 2015). Both modelling efforts (e.g. Langebroek and Nisancioglu, 2014) and data compilations (Capron et al., 2014) show a shift in patterns of regional temperature changes, possibly linked to significant differences in insolation changes at different latitudes (see Fig. 1 in Langebroek and Nisancioglu, 2014) during the Eemian. One of the major questions that arises from these studies is how to distinguish between contributions from the Greenland and Antarctic ice sheets to Eemian sea-level change, specifically in terms of timing and magnitude. The use of a coupled ice-sheet – sea-level model can help address this issue due to its ability to link climate variations to RSL change via ice sheet dynamics (e.g. Rovere et al., 2016).

Here, we show data for four different locations as described in Long et al. (2015) (Fig. 6). As can be seen, the Eemian is characterised by a rise in sea level following the penultimate glacial maximum that culminates in a RSL peak above present at all four sites considered. Differences between the records shown in Fig. 6 include differences in the timing and rate of the rise in sea level, the maximum sea-level high stand, and the possible double peak of sea level with a short interval of lower RSL during the Eemian (Dutton et al., 2015). The interpretation of the data involves some challenges, particularly in terms of determining the precise age and measurement uncertainty and correcting for processes such as GIA and tectonics (Rovere et al., 2016).

3.2. Last Glacial Maximum to the present

The LGM is characterised by a global mean cooling of ~ 4.0 ± 0.8 °C (Annan and Hargreaves, 2013) and it refers to the

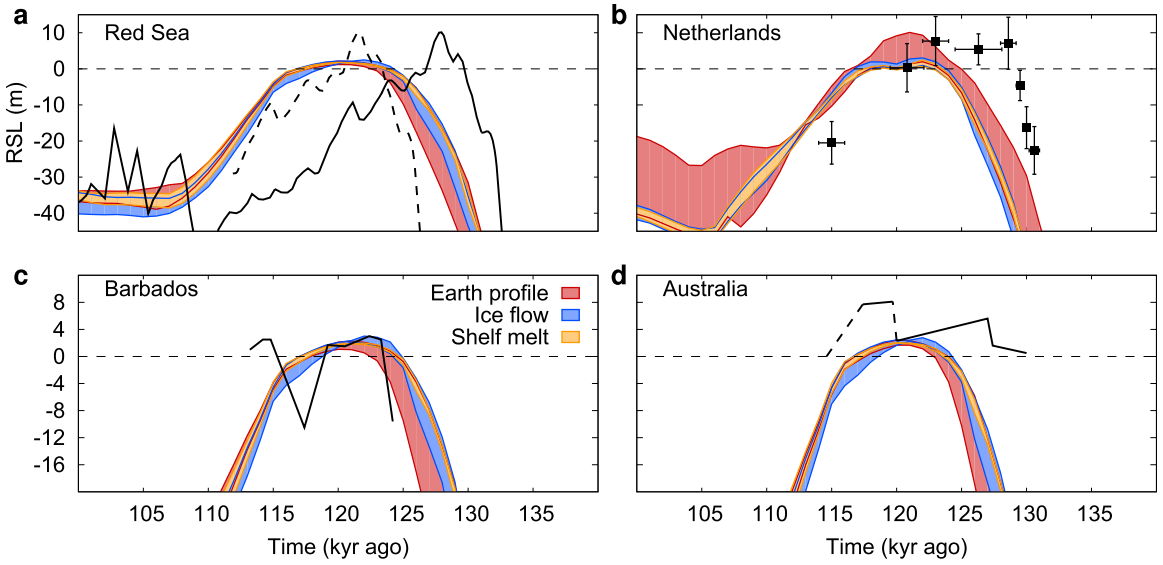

Fig. 6. A comparison of multiple runs of ANICE-SELEN (De Boer et al., 2014) as described in Table 1 with different RSL data from the Eemian. Each colour band represents the range of a particular suite of experiments for each location, and each band is bounded by the lines that represent the maximum and minimum value of each experiment. Note that the colour bands overlap. Red: rheological Earth profile is varied. Blue: ice flow parameter is varied. Orange: sub-shelf melt parameter is varied. The RSL data reflect sea-level change at four distinct sites: a) The Red Sea, using the age models of Rohling et al. (2008) (dashed black line) and Grant et al. (2012). b) The Netherlands: corrected data for compaction, tectonics and differential isostasy (Lambeck et al., 2006). c) Barbados (Thompson and Goldstein, 2005) and d) Australia (O'Leary et al., 2013). Curves as adopted from Long et al. (2015).

maximum glacial extent (~ 19–26 kyr ago (Clark et al., 2009)) of the last glacial cycle that starts after the Eemian. During the LGM large ice sheets covered the northern hemisphere (NH) (Peltier, 2004; Ehlers and Gibbard, 2007), with major ice sheets centred on North America (e.g. Tarasov et al., 2012) and Eurasia (e.g. Hughes et al., 2016), and the AIS extended towards the edge of the continental shelf (e.g. Bentley et al., 2014; Briggs et al., 2014). The growth of these ice sheets contributed to a global mean sea level minimum, relative to the present, of about 130 m during the LGM (e.g. Peltier and Fairbanks, 2006; Clark et al., 2009; Lambeck et al., 2014). The vast glacial extent seen during the LGM was accompanied by significant temperature decreases in the regions where ice sheets were present (NGRIP members, 2004; Jouzel et al., 2007; Annan and Hargreaves, 2013) and a drop in CO_2 concentrations down to ~ 185 ppmv (Petit et al., 1999).

In this study, we consider RSL change around the Antarctic continent (Briggs et al., 2013) at four near-field sites. In contrast to the rapid rise in RSL recorded at far-field sites around the world for this period, data from the Antarctic sites shows a drop in RSL between 12 kyr ago and the present due to the proximity of the sites to regions of local ice mass loss (Fig. 7). Differences between the records reflect differences in the precise glacial extent during the LGM and timing of the retreat following the LGM at different locations around the continent (Bentley et al., 2014).

4. Model-data comparison

In terms of comparing models with data, several different approaches can be employed. One approach involves identifying which reconstruction of ice volume and extent provides the optimal fit to observations of past sea level, ice extent or ice thickness; this has been done in the past for e.g. Fennoscandia (Lambeck et al., 1998) and Greenland (Tarasov and Peltier, 2003; Simpson et al., 2009). An extension of this approach involves the use of data assimilation methods to ensure the optimum fit to the observational constraints (Stuhne and Peltier, 2015). Alternatively, an ensemble approach has been used to produce a suite of reconstructions of, e.g. the North American ice sheet (Tarasov and Peltier, 2004), and the AIS (Whitehouse et al., 2012b; Briggs et al., 2014; Pollard et al., 2016). Tarasov et al. (2012) extend this approach to include the use of Bayesian calibration within an ensemble framework. In these studies different model parameters are varied to generate a large ensemble of model simulations which are then compared with the observations using statistical measures (as given by e.g. Briggs et al., 2013; Pollard et al., 2016). A more integrated approach has also recently been employed in which an ice-sheet model is iteratively tuned to fit observational data associated with the last deglaciation of Greenland. In this case the complete model, i.e. the ice-sheet model and then the GIA model, are re-run several times (Lecavalier et al., 2014).

One issue that cannot be addressed by these individual ice-sheet reconstructions is the question of whether it is possible to account for temporal variations in global ice volume, as inferred from far-field sea-level records (Lambeck et al., 2014). This is the goal of the global ICE-NG reconstructions of ice volume, where the most recent examples are the ICE-5G (Peltier, 2004) and ICE-6G_C (Peltier et al., 2015) models.

As highlighted in the review of Stokes et al. (2015) the different approaches to reconstructing past ice sheets, and thus sea level, have both strengths and weaknesses. With the traditional GIA approach, ice sheet reconstructions are constrained using ice extent data, RSL data and observations of present-day uplift. However, the resulting ice-sheet history will not necessarily be consistent with glaciological flow models and their underlying physics. Conversely, when sophisticated ice-sheet models are used the results will be consistent with the physics governing the laws of ice flow, but may not fit data relating to past ice extent or sea-level change. Moreover, it is not currently possible to force long-term ice-sheet simulations with realistic simulations of past climate, since it is not yet computationally feasible to run general circulation models for long periods of time at sufficiently high resolution (Stokes et al., 2015). As a consequence, mass balance forcing of ice-sheet models is usually accounted for in a highly parameterised way (e.g. Pollard and DeConto, 2012; De Boer et al., 2013).

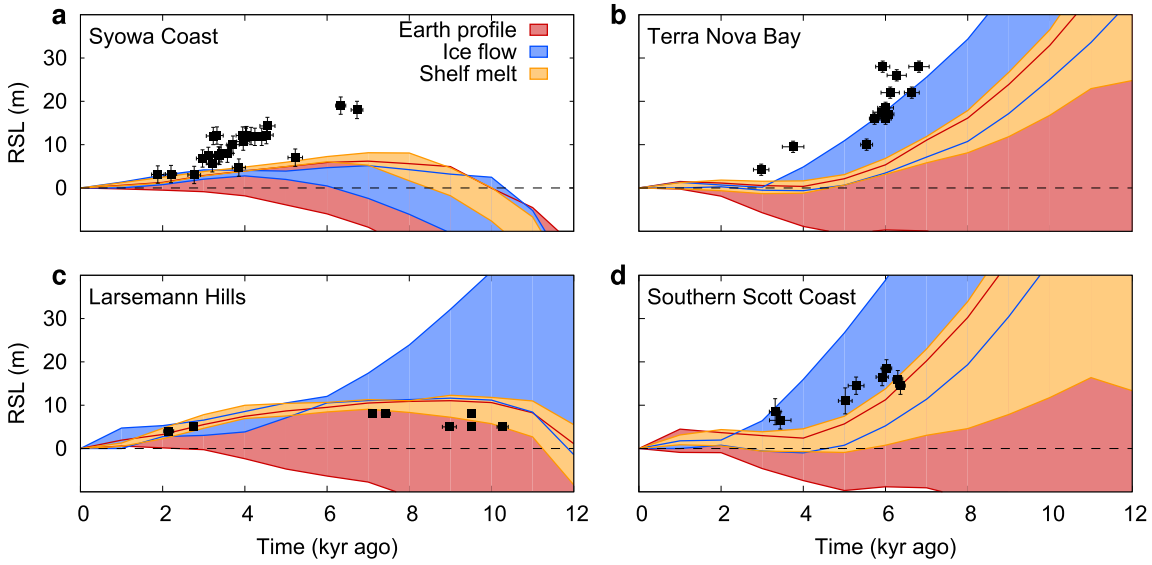

Fig. 7. A comparison of multiple runs with ANICE-SELEN (De Boer et al., 2014) as described in Table 1 with different RSL data from Antarctica. Each colour band represents the range of a particular suite of experiments for each location, and each band is bounded by the lines that represent the maximum and minimum value of each experiment. Note that the colour bands overlap. Red: rheological Earth profile is varied. Blue: ice flow parameter is varied. Orange: sub-shelf melt parameter is varied. The RSL data reflect sea-level change at four distinct sites: a) Syowa Coast, b) Terra Nova Bay, c) Larsemann Hills and d) Southern Scott Coast. Data from the compilation of Briggs et al. (2013).

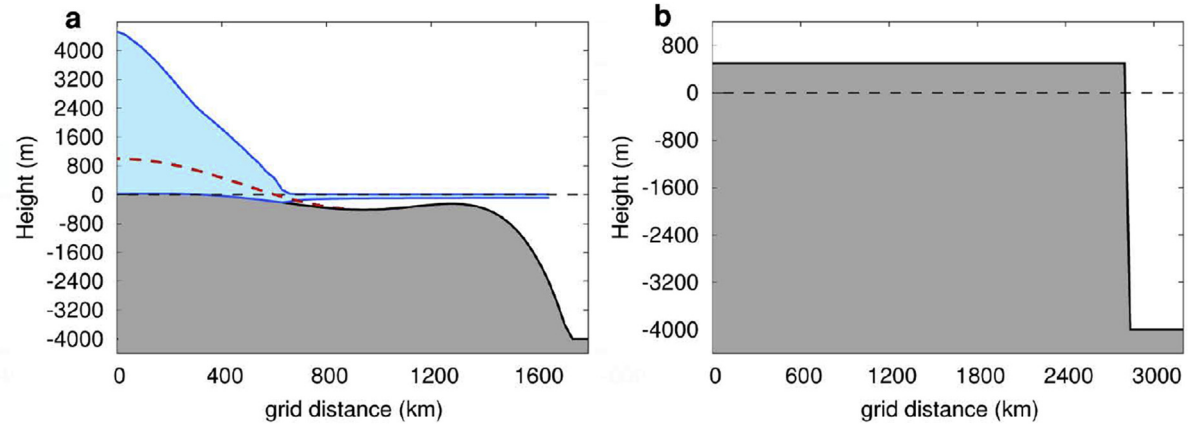

Fig. 8. Cross sections of the ice-sheet regions used for the schematic experiment. a) The ice sheet in the SH, which evolves through time. The blue-filled shape indicates the ice sheet after a 20 kyr steady state spin up. The red dashed line represents the initial bedrock topography (see text for details). b) Initial NH topography: a circular continent with a constant elevation of 500 m above sea level and a radius of 2800 km. Both regions are axisymmetric around the South and North Pole, respectively.

One of the advantages of simultaneously modelling global ice volume and RSL change using a coupled ice-sheet – sea-level model is that a direct comparison with geological data (e.g. RSL, ice extent and ice thickness data) can be carried out within a more self-consistent framework. We performed a number of sensitivity tests with the coupled ice-sheet – sea-level model ANICE-SELEN of De Boer et al. (2014) and compare the resulting suite of model realisations with RSL data from around the world (Figs. 6 and 7). The sensitivity tests detailed here provide a general example of the parameters that can be varied within a coupled model. We vary: (i) lithospheric thickness and the viscosity of the mantle (e.g. Whitehouse et al., 2012b) (ii) the enhancement factors for ice flow of ice streams and floating ice (e.g. Maris et al., 2014), and (iii) a melt parameter governing ice-shelf basal melt rates (e.g. Stone et al., 2013; Fitzgerald et al., 2012). The different values for each of the above named variables that we have used are shown in Table 1.

Although we only carry out a first-order comparison, similar to Whitehouse et al. (2012b) and Gomez et al. (2013), it is clear that there are certain locations where a subset of the model realisations - noting that each colour band in Figs. 6 and 7 represents the range for one of the experiments given in Table 1 - fit the RSL data better than others. Our model is forced by the LR04 benthic δ^{18} O curve (Lisiecki and Raymo, 2005), but, as illustrated in Fig. 6a, the revised dating of the Red Sea RSL record (Grant et al., 2012) leads to an offset between our model predictions and the observations. In addition, the magnitude of peak sea level during the last interglacial is not reproduced by the model at this location. For the Netherlands (Fig. 6b), the runs in which the Earth rheology is varied (red) are able to reproduce the maximum observed sea level, but again there is an offset in the timing. Furthermore, the double peak that is seen in the data from Barbados (Fig. 6c) and Australia (Fig. 6d) is not featured at all in the model simulations, which could be ascribed to missing inter hemispheric differences in temperature (Capron et al., 2014; Langebroek and Nisancioglu, 2014).

When considering post-LGM near-field RSL change around

Table 1
Sensitivity tests with the coupled ice-sheet – sea-level model ANICE-SELEN described in De Boer et al. (2014). For the viscosity we employed a 3-layer 1-D Maxwell Earth model with a Lower mantle (L), Transition zone (T) and an Upper mantle (U). The results of these tests are illustrated in Figs. 6 and 7, with the range of each experiment shown in red for the Earth profile, in blue for the ice flow parameter, and in orange for the shelf melt experiments.

Test	variable	values
Earth profile	Lithosphere thickness & viscosity (L; T; U)	65 km, 1; 0.2; 0.1 × 10^{21} Pa s 96 km, 3; 1;0.5 × 10^{21} Pa s 120 km, 50; 10; 5 × 10^{21} Pa s
Ice flow	Enhancement factor for SSA velocities	0.1 0.5 0.9
Shelf melt	Sub-shelf melt parameter	1 × 10^{-3} 2.5 × 10^{-3} 10 × 10^{-3}

Antarctica (Fig. 7), the different sensitivity tests lead to a large spread in the model results: for Terra Nova Bay (Fig. 7b) and Southern Scott Coast (Fig. 7d) the runs in which ice flow parameters are varied (blue) are able to fit the data, but these same model simulations show a large offset to data from the Larsemann Hills (Fig. 7c). The simulations with varying ice flow (blue) and shelf melt (orange) seem to represent the data from the Larsemann Hills (Fig. 7c) better, whereas none of the model realisations fully represent the drop in RSL shown by the data from the Syowa Coast (Fig. 7a). This first-order comparison already indicates that it can be a challenging task to fit model results to observations (e.g. Whitehouse et al., 2012b; Briggs et al., 2014). However, in future attempts to simultaneously simulate ice volume and RSL change, observational data could be used to reconfigure the model as it runs (e.g. as done in Stuhne and Peltier, 2015), although the need to run the model multiple times is still required to establish the initial topography.

5. Schematic experiments for ice-sheet – sea-level models

In this section we present a schematic example of a coupled ice-sheet – sea-level simulation that could potentially form the basis of a future coupled model benchmarking exercise. We focus on the implications of using spatially-variable, model-derived RSL change instead of global mean sea level to drive an ice-sheet model that predicts the evolution of ice volume over a glacial cycle, a period for which it has previously been demonstrated that sea-level feedbacks can significantly alter ice-sheet evolution (Gomez et al., 2013; De Boer et al., 2014).

5.1. Experimental design

Our model domain encompasses the whole Earth, and we consider two polar land masses which are surrounded by a 4000-m deep ocean, similar to the set up used in Gomez et al. (2012). The initial bedrock topography of the southern polar continent is axisymmetric, and is based on Gudmundsson et al. (2012):

$$H_b(r) = b_0 - c_1\left(\frac{r}{r_0}\right)^2 + c_2\left(\frac{r}{r_0}\right)^4 - c_3\left(\frac{r}{r_0}\right)^6, \quad (4)$$

where r is the radius from the south pole in metres, all parameters are given in Table 2. The initial topography is illustrated by the dashed line in Fig. 8a. We calculate the ice-sheet changes in the southern hemisphere (SH) using the ice-sheet model ANICE, forced by either spatially-variable or global mean sea-level change. The ice-sheet model combines ice flow calculations based on the SIA and SSA (De Boer et al., 2013, 2014). For simplicity, we consider vertically averaged velocities, using a single value for the ice-flow parameter (see Table 2). Similarly, surface mass balance is kept simple and we use a single value for accumulation of 0.4 m yr^{-1}. For the basal friction we use a Mohr-Coulomb plastic law, with basal stresses included in the SSA equations. Basal stress is assumed to be a function of a till yield stress τ_c that spatially varies as a function of bedrock elevation (De Boer et al., 2013):

$$\tau_c = tan(\phi)(1 - 0.96\lambda)\rho_i g H_i. \quad (5)$$

Here, ϕ is the till friction angle, with a lower and upper limit depending on bedrock elevation as given in Table 2. The factor λ is a scaling function of the pore water pressure depending on bedrock elevation, λ is 1 below sea level and it is linearly scaled down to 0 for bedrock 1000 m above sea level.

The land mass in the NH consists of a circular continent of radius 2800 km centred on the North Pole, which has a fixed height of 500 m (Fig. 8b). The ice sheet in the NH is assumed to be cylindrical, with a radius of 2500 km and a thickness that is prescribed to vary between 0 (glacial index = 0) and 4400 m (glacial index = 1) (Fig. 9a), the latter being equivalent to a global mean sea-level reduction of about 140 m. Global sea-level changes are driven by output from the SH ice-sheet model and the prescribed changes to the NH ice sheet.

The SLE is solved with SELEN. The solid Earth is represented by a 1-D Maxwell Earth model with 3 viscous layers (Table 2), rheological parameters are similar to those used in De Boer et al. (2014). The pseudo-spectral method is used to solve the SLE to a maximum spherical harmonic degree of 128. The only forcing for the experiment is the glacial index as illustrated in Fig. 9a, which drives the

Table 2
Model parameters for the schematic experiments.

Constant & description		value
ρ_i	Ice density (kg m^{-3})	910
ρ_w	Seawater density (kg m^{-3})	1028
g	Gravity acceleration (m s^{-1})	9.81
A_{flow}	Ice-flow parameter (Pa^{-3} s^{-1})	1 × 10^{-24}
a	Surface accumulation (m yr^{-1})	0.4
ϕ	Till friction angle (°)	5 to 15
$H_{b\phi}$	Bedrock height limits (m)	-200 to 500
b	Optional basal melt (m yr^{-1})	0.0
L	Lithosphere thickness (km)	100
n	Number of visco-elastic layers	3
visc(1)	Upper mantle viscosity (Pa s)	3 × 10^{20}
visc(2)	Transition zone viscosity (Pa s)	6 × 10^{20}
visc(3)	Lower mantle viscosity (Pa s)	3 × 10^{21}
b_0	Central bedrock height (m)	1000
c_1	Contour parameter 1 (m)	2148.8
c_2	Contour parameter 2 (m)	1031.72
c_3	Contour parameter 3 (m)	151.72
r_0	Scaling radius (m)	750000

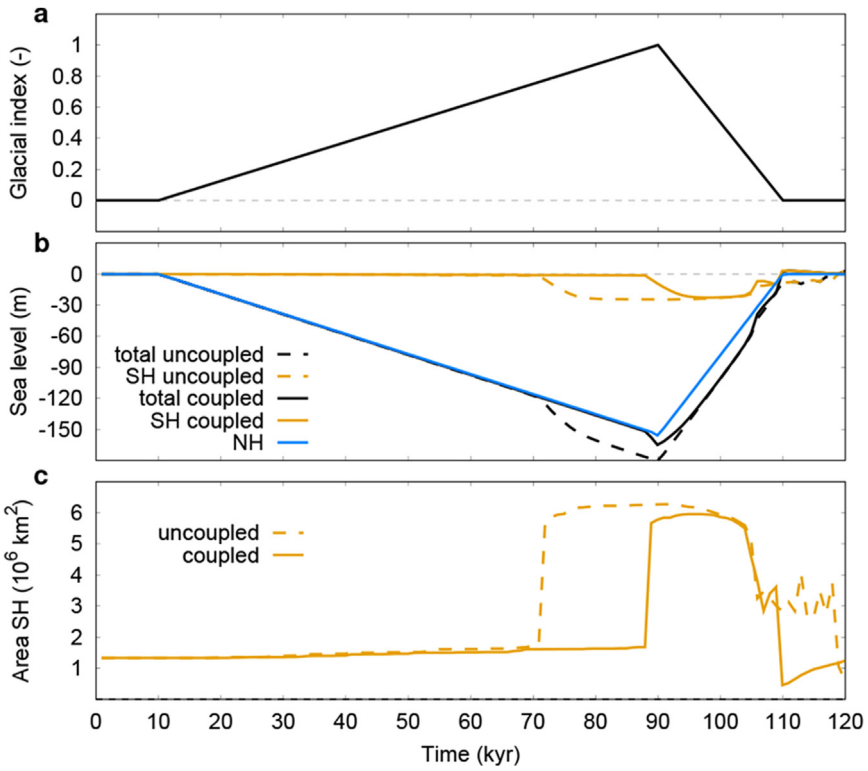

Fig. 9. Results from the schematic experiments. a) The glacial index used to drive the NH ice volume. b) Sea level contributions from the ice sheets, with solid lines for the coupled (using RSL) and dashed lines for the uncoupled (using global mean sea level) simulations. Total in black, NH in blue, SH in orange. c) SH ice sheet area, solid for the coupled simulation, dashed for the uncoupled simulation. Note that the sea-level contribution from the NH ice sheet is the same for the two experiments, since this is driven by the glacial index in panel (a).

NH ice volume and hence sea level. The SH ice sheet is first spun up to an initial state as illustrated in Fig. 8a, with no change in NH ice volume. All sea-level contributions are calculated relative to this initial ice sheet, hence a sea-level change from the SH ice sheet of 0 means that the ice sheet does not change relative to its initial state after spin up.

5.2. Results of the schematic experiments

We perform a full glacial experiment starting with the initial conditions shown in Fig. 8. The glacial index (Fig. 9a) drives the NH ice volume to a maximum drop of ~ 140 m global mean sea level, as shown by the blue curve in Fig. 9b. When using the uncoupled model (dashed orange lines) the growth of the SH ice sheet starts much earlier during the glacial cycle (soon after 70 kyr into the simulation) compared with the scenario that uses the coupled model (solid orange lines). Although the SH ice sheet in both simulations reaches a similar volume (Fig. 9b) and ice extent (Fig. 9c), the coupled simulations predict earlier deglaciation of this ice sheet compared with the uncoupled simulations that are driven by global mean sea level.

Fig. 10 shows cross sections over the south polar region from 90 to 50 °S at 0, 70, 80 and 95 kyr into the simulation. The height of the sea-surface is different in the two simulations in the near-field of the ice-sheets; the sea surface height in the coupled simulation (solid orange line) is perturbed upwards in the region of increased ice mass, whereas the sea-surface height in the uncoupled simulation (dashed orange line) just follows the global mean sea-level change. The increase in SH ice volume in the uncoupled simulation (red shape in Fig. 10c) is accompanied by a strong decrease in bedrock deformation and a drop in the global mean sea-surface height. In contrast, due to self-gravitational effects the sea-surface height in the near field of the ice sheet slightly increases in the coupled simulation (orange solid line in Fig. 10d). In conclusion, similar to the results presented in earlier papers (Gomez et al., 2013; De Boer et al., 2014), we find that advance and retreat of a marine ice-sheet system can be strongly perturbed by the inclusion of self-gravitational effects.

6. Future perspectives

The factors discussed in Section 2 are relatively straightforward to implement in current ice-sheet – sea-level models. In this section we discuss some of the outstanding challenges associated with the implementation of coupled ice-sheet – sea-level models and address key mechanisms that should be taken into account in future (versions of) ice-sheet – sea-level models.

6.1. Grounding-line migration

When accounting for the change in the ocean area as discussed in Section 2.2, the interaction of the grounding-line position of the ice sheets with the local RSL change is an essential process that requires specific attention in future ice-sheet models. Currently the majority of coupled ice-sheet – sea-level models make use of an ice-sheet model that uses the SIA and SSA to simulate ice flow (Gomez et al., 2013; De Boer et al., 2014; Konrad et al., 2015). Although these types of models are well suited to simulating long-term changes in ice volume, a proper treatment of grounding-line migration for lower resolution models requires additional parameterisations (Pattyn et al., 2013; Feldmann et al., 2014), especially when focusing on short-term future projections.

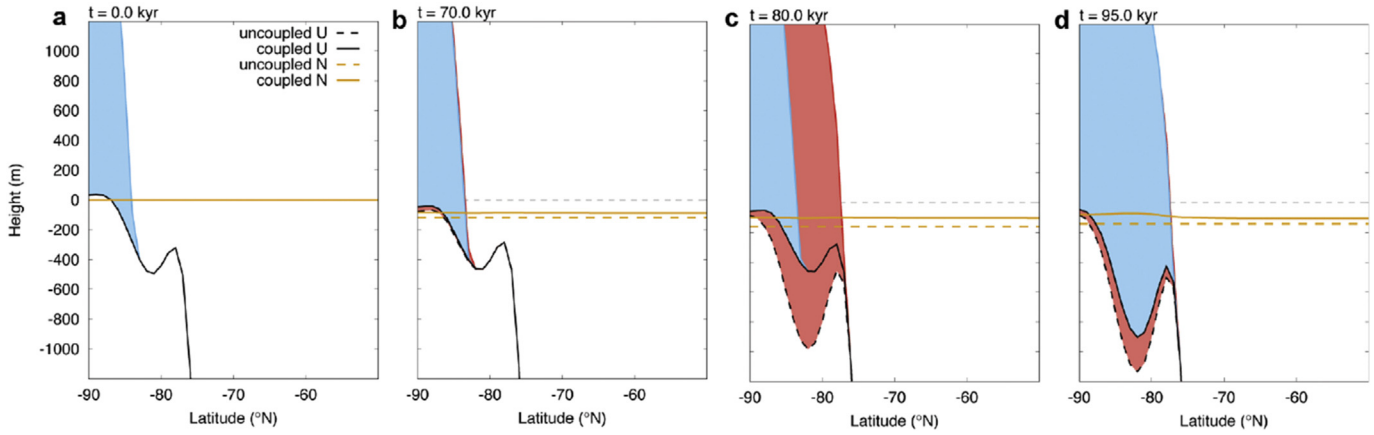

Fig. 10. Results from the schematic experiments for four time slices. A zoomed in and zonal mean cross section over the south polar region showing the SH ice sheet (blue shading for the coupled simulation, and red shading for the uncoupled simulation), bedrock elevation U (black) and sea surface height N (orange). Solid lines represent the coupled simulation, dashed lines the uncoupled simulation. a) the initial conditions at the start of the simulation. b) After 70 kyr, c) after 80 kyr, the SH ice sheet has grown in the uncoupled simulation (red shading), d) after 95 kyr, both simulations now show a larger SH ice sheet. In all panels the reference height ($z = 0$) is shown with a horizontal dashed grey line.

6.2. Lateral variation in Earth's rheology

As demonstrated by Gomez et al. (2013, 2015) and Konrad et al. (2015), the choice of Earth model can significantly alter the ice-sheet evolution predicted by a coupled ice-sheet – sea-level model. In future studies it will therefore be important to take into account any lateral variations in Earth properties that exist beneath an ice sheet. However it is first important to quantify the impact of lateral variations, because 3-D GIA models are computationally (on the order of 100 times) more expensive than models that just assume a radially-varying Earth structure. 3-D GIA models, which prescribe both lateral and vertical variations in Earth rheology, have been used for a number of years to study a wide range of applications (e.g. Latychev et al., 2005; Whitehouse et al., 2006; Kendall et al., 2006; Austermann et al., 2013; Van der Wal et al., 2013, 2015). Particularly relating to this study, we note that across Antarctica there are large spatial variations in Earth properties across the continent (e.g. Morelli and Danesi, 2004; Hansen et al., 2014; An et al., 2015; Heeszel et al., 2016).

Ice mass change in areas that are thought to be underlain by a weak upper mantle can trigger a large, and almost instantaneous solid Earth response (Nield et al., 2012, 2014), which can help to stabilise the ice-sheet system (Gomez et al., 2015; Konrad et al., 2015). It is important to identify such regions, e.g. using seismic data, and to determine the resolution at which spatial variations should be represented within the Earth model - there will be a balance between running high resolution, computationally-expensive experiments, and acknowledging that some small scale details will be 'invisible' to the surface loading. When solving for GIA and RSL there is always the need to represent the whole Earth, for the 3-D case efficiency can be gained by using finite element models with a mesh of varying resolution.

6.3. Effects of deposition of sediment

Over longer timescales of 10,000–100,000 years, coupled models will need to account for erosion and deposition of sediment (Dalca et al., 2013), particularly in areas periodically covered by large ice sheets. This is important because large-scale sediment redistribution will influence the regional isostatic response, and because the underlying topography exerts a strong control on ice dynamics (Jamieson et al., 2012). Moreover other processes related to landscape evolution, such as dynamic topography, will also be important when accounting for the interaction between ice sheets and sea level over these long time scales (Austermann et al., 2015).

6.4. Improving computational efficiency

An important point raised in Section 2.3 is the computational cost of solving the viscoelastic SLE over long time scales. In order to reduce the computation time and increase the spatial and spectral resolution across the ice sheets we have implemented parallelisation of the SELEN code that solves the SLE and a scheme that generates a heterogeneous mesh.

6.4.1. Parallel programming

The original SELEN code is based on a typical top-down serial algorithm, where the calculation of the SLE itself is the slowest process (Spada and Stocchi, 2007). Since it uses the pseudo–spectral method (Mitrovica and Peltier, 1991) and since all variables are discretised, the multiple nested do-loops, which cycle through harmonic degree, time and space, can be parallelised. Here, we take advantage of the Open MP (Open Multi–Processing) application programming interface in order to parallelise the multiple nested do-loops. Accordingly, any time a do-loop is encountered, the master thread is divided into parallel threads that are directed to different cores. Each core performs a part of the spatio-temporal convolutions. Afterwards, the output is re-assembled into one array by means of reduction.

6.4.2. Heterogeneous mesh

For the heterogeneous mesh, we take advantage of the pixelisation routine (Tegmark, 1996) that, according to the *RES* parameter (equation (3)), first finds the main latitudes and then generates hexagonal elements around them. This allows for a mesh where the resolution (i.e. the area of hexagons) depends on the latitude only. This is very convenient because continental ice sheets, where higher spatial resolution is needed, are typically located at high latitudes, while the rest of the Earth, where a lower resolution would be sufficient, is mostly covered by deep oceans. Firstly, we choose the *RES* value for the higher resolution elements and generate a high resolution global mesh accordingly. Secondly, we generate other meshes for smaller *RES* values. The maximum degree of the analysis (l_{max}) must be such that $N_P^{min} \geq l_{max}^2/3$ to take

advantage of the "window property" of the pixelisation, which ensures that the orthonormality condition of the spherical harmonics holds numerically (Tegmark, 1996). Since l_{max} is set to match the high resolution mesh, the *RES* value of the coarser mesh must be chosen carefully. Lastly, once the meshes are generated, a criterion can be adopted to create a hybrid mesh consisting of the different elements. The highest-resolution elements are used at the poles and the lower resolution elements around the equator. Once the hybrid mesh is created, the actual topography can be projected onto the hexagons. It is important, at this point, to evaluate the ratio between the total number of the elements in each mesh. Such a value is then used as a multiplicative factor when computing the spherical harmonic expansion for the ocean function.

6.4.3. Schematic examples of a reduction in computation time

Similar to the schematic experiment presented above, we also consider a hypothetical scenario where the initial topography now consists of two circular and flat continents at the poles that are separated by an ocean. The continents have a 20° radius and an initial elevation of 20 m above sea level. The bathymetry increases stepwise towards lower latitudes and reaches a value of −200 m between 50°S and 50°N. The topography is interpolated using a hybrid mesh that consist of two classes of hexagonal elements. Higher resolution elements (*RES* = 60), with a grid distance of ∼ 48 km, are used in the northern hemisphere between 50 and 90°N, while lower resolution elements (*RES* = 15), with a grid distance of ∼ 196 km, are used below 50°N. A uniform thickness disk of ice is placed at the north pole. The disk has a radius of 18° and it is discretised into high-resolution hexagonal elements (*RES* = 60). The thickness of the disk of ice increases linearly to 2000 m in 100 kyr and decreases back to 0 in the following 20 kyr. The tests discussed in this particular section are carried out using the stand-alone sea-level code of SELEN, not coupled to an ice-sheet model.

To compare the different approaches used to reduce computational costs we have run three different simulations: (i) a *standard* simulation with *RES* = 60, (ii) a *parallel* simulation with parallelised do-loops, and (iii) a simulation that combines the parallel code and the heterogeneous mesh (*parallel* + *het.mesh*). The computation times for these three experiments are very different. The *standard* simulation takes about 20 h, while the *parallel* and *parallel* + *het.mesh* simulations take 10 and 2.5 h, respectively. The results for the *standard* and *parallel* simulations are identical, whereas differences in RSL between the *standard* and *parallel* + *het.mesh* simulations peak at ∼ 0.4 m (Fig. 11). The greatest differences are seen around the margin of the southern hemisphere continent. Here, the larger-size mesh elements result in a less optimal discretisation of the bathymetry. Accordingly, the pressure exerted by the water load on the seafloor is different during regressions and transgression. Other differences can be seen in the northern hemisphere around 50°N, where a sudden transition from high-resolution to low-resolution elements occurs.

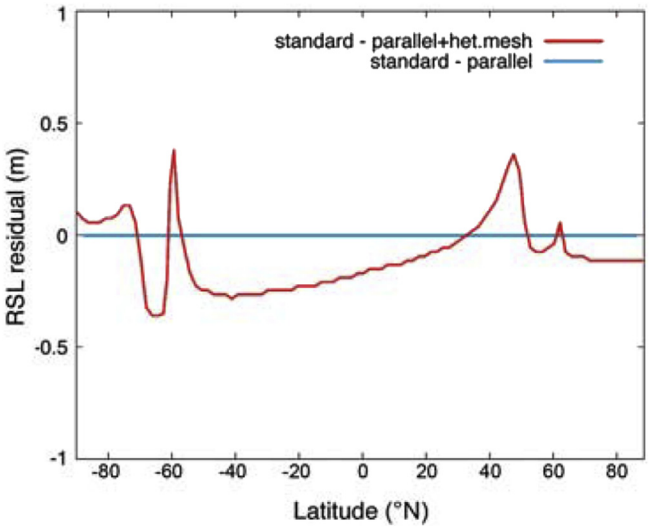

Fig. 11. Residual RSL change at the glacial maximum, after 100 kyr of simulation. The cyan line shows along-meridian difference between the *standard* and *parallel* predictions, zero everywhere. The red curve shows the difference between *standard* and *parallel* + *het.mesh* predictions.

7. Conclusions

In this article we discuss the importance of integrating two previously-separate fields of research: Glacial Isostatic Adjustment and ice sheet dynamics. Specifically, over past glacial cycles the incorporation of self gravitational effects is shown to play an important role in modulating rates of ice-sheet advance and retreat. In particular, it has been shown that RSL change can act to stabilise marine ice-sheet retreat, even on a retrograde bed, depending on the specific Earth rheology and climate scenario applied. The field of coupled ice-sheet − sea-level modelling is still relatively young. Future work in this area should seek to: (i) improve model representations of grounding-line migration, (ii) account for lateral variations in Earth's rheology, and (iii) improve the computational efficiency of the models. Progress over the last few years has shown that a consistent ice-sheet − sea-level model is not only feasible, but that coupled ice-sheet − sea-level models have an important role to play in improving our understanding of the interactions between sea-level change and ice-sheet dynamics, during both past and future climate changes.

Acknowledgements

We thank the editors at QSR for inviting this review, and Lev Tarasov and an anonymous reviewer for their constructive reviews that improved the manuscript. B. de Boer acknowledges funding from the European Union's Horizon 2020 research and innovation programme under the Marie Sklodowska-Curie grant agreement No 660814 and is currently funded by NWO Earth and Life Sciences (ALW), project 863.15.019. Model simulations were undertaken on ARC2, part of the High Performance Computing facilities at the University of Leeds, UK. P.L. Whitehouse is funded by a NERC Independent Research Fellowship (NE/K009958/1). We would like to thank Natalya Gomez for providing model output. We thank Natasha Barlow for discussion on the sea level curves for the last interglacial. Model output, specifically for the schematic experiments, is available upon request.

References

Adhikari, S., Ivins, E.R., Larour, E., 2016. ISSM-SESAW v1.0: mesh-based computation of gravitationally consistent sea-level and geodetic signatures caused by cryosphere and climate driven mass change. Geosci. Model Dev. 9, 1087–1109. http://dx.doi.org/10.5194/gmd-9-1087-2016.

An, M., Wiens, D.A., Zhao, Y., Feng, M., Nyblade, A.A., Kanao, M., Li, Y., Maggi, A., LÈvíque, J.J., 2015. S-velocity model and inferred Moho topography beneath the Antarctic plate from rayleigh waves. J. Geophys. Res. Solid Earth 120, 359–383. http://dx.doi.org/10.1002/2014JB011332.

Annan, J.D., Hargreaves, J.C., 2013. A new global reconstruction of temperature changes at the Last Glacial Maximum. Clim. Past 9, 367–376.

Argus, D.F., Peltier, W.R., Drummond, R., Moore, A.W., 2014. The Antarctica component of postglacial rebound model ICE-6G_C (VM5a) based on GPS positioning, exposure age dating of ice thicknesses, and relative sea level histories. Geophys. J. Int. 198, 537–563. http://dx.doi.org/10.1093/gji/ggu140.

Austermann, J., Mitrovica, J.X., Latychev, K., Milne, G.A., 2013. Barbados-based estimate of ice volume at Last Glacial Maximum affected by subducted plate.

Mature Geosci. 7, 553–557.
Austermann, J., Pollard, D., Mitrovica, J.X., Moucha, R., Forte, A.M., DeConto, R.M., Rowley, D.B., Raymo, M.E., 2015. The impact of dynamic topography change on Antarctic ice sheet stability during the mid-Pliocene warm period. Geology 43, 927–930.
Bentley, M.J., ÓCofaigh, C., Anderson, J.B., Conway, H., Davies, B., Graham, A.G.C., Hillenbrand, C.D., Hodgson, D.A., Jamieson, S.S.R., Larter, R.D., Mackintosh, A., Smith, J.A., Verleyen, E., Ackert, R.P., Bart, P.J., Berg, S., Brunstein, D., Canals, M., Colhoun, E.A., Crosta, X., Dickens, W.A., Domack, E., Dowdeswell, J.A., Dunbar, R., Ehrmann, W., Evans, J., Favier, V., Fink, D., Fogwill, C.J., Glasser, N.F., Gohl, K., Golledge, N.R., Goodwin, I., Gore, D.B., Greenwood, S.L., Hall, B.L., Hall, K., Hedding, D.W., Hein, A.S., Hocking, E.P., Jakobsson, M., Johnson, J.S., Jomelli, V., Jones, R.S., Klages, J.P., Kristoffersen, Y., Kuhn, G., Leventer, A., Licht, K., Lilly, K., Lindow, J., Livingstone, S.J., Massé, G., McGlone, M.S., McKay, R.M., Melles, M., Miura, H., Mulvaney, R., Nel, W., Nitsche, F.O., O'Brien, P.E., Post, A.L., Roberts, S.J., Saunders, K.M., Selkirk, P.M., Simms, A.R., Spiegel, C., Stolldorf, T.D., Sugden, D.E., van der Putten, N., van Ommen, T., Verfaillie, D., Vyverman, W., Wagner, B., White, D.A., Witus, A.E., Zwartz, D., 2014. A community-based geological reconstruction of antarctic ice sheet deglaciation since the Last Glacial Maximum. Quat. Sci. Rev. 1–9.
Bindschadler, R.A., Nowicki, S., Abe-Ouchi, A., Aschwanden, A., Choi, H., Fastook, J., Granzow, G., Greve, R., Gutowski, G., Herzfeld, U., Jackson, C., Johnson, J., Khroulev, C., Levermann, A., Lipscomb, W.H., Martin, M.A., Morlighem, M., Parizek, B.R., Pollard, D., Price, S.F., Ren, D., Saito, F., Sato, T., Seddik, H., Seroussi, H., Takahashi, K., Walker, R., Wang, W.L., 2013. Ice-sheet model sensitivities to environmental forcing and their use in projecting future sea level (the SeaRISE project). J. Glaciol. 59, 195–224.
Bintanja, R., Van de Wal, R., 2008. North American ice-sheet dynamics and the onset of 100,000-year glacial cycles. Nature 454, 869–872.
Bradley, S.L., Milne, G.A., Shennan, I., Edwards, R., 2011. An improved glacial isostatic adjustment model for the British Isles. J. Quat. Sci. 26, 541–552. http://dx.doi.org/10.1002/jqs.1481.
Briggs, R., Pollard, D., Tarasov, L., 2013. A glacial systems model configured for large ensemble analysis of Antarctic deglaciation. Cryosphere 7, 1949–1970.
Briggs, R.D., Pollard, D., Tarasov, L., 2014. A data-constrained large ensemble analysis of Antarctic evolution since the Eemian. Quat. Sci. Rev. 103, 91–115. http://dx.doi.org/10.1016/j.quascirev.2014.09.003.
Bueler, E., Brown, J., 2009. Shallow shelf approximation as a "sliding law" in a thermomechanically coupled ice sheet model. J. Geophys. Res. 114.
CAPE Last Interglacial Project Members, 2006. Last Interglacial Arctic warmth confirms polar amplification of climate change. Quat. Sci. Rev. 25, 1383–1400.
Capron, E., Govin, A., Stone, E.J., Masson-Delmotte, V., Mulitza, S., Otto-Bliesner, B., Rasmussen, T.L., Sime, L.C., Waelbroeck, C., Wolff, E.W., 2014. Temporal and spatial structure of multi-millennial temperature changes at high latitudes during the last interglacial. Quat. Sci. Rev. 103, 116–133. http://dx.doi.org/10.1016/j.quascirev.2014.08.018.
Clark, J.A., Farrell, W.E., Peltier, W.R., 1978. Global changes in postglacial sea level: a numerical calculation. Quat. Res. 9, 265–287.
Clark, P.U., Dyke, A.S., Shakun, J.D., Carlson, A.E., Clark, J., Wohlfarth, B., Mitrovica, J.X., Hostetler, S.W., McCabe, A.M., 2009. The Last Glacial Maximum. Science 325, 710–714.
Cornford, S.L., Martin, D.F., Graves, D.T., Ranken, D.F., Le Brocq, A.M., Gladstone, R.M., Payne, A.J., Ng, E.G., Lipscomb, W.H., 2013. Adaptive mesh, finite volume modeling of marine ice sheets. J. Comput. Phys. 232, 529–549. http://dx.doi.org/10.1016/j.jcp.2012.08.037.
Dalca, A.V., Ferrier, K.L., Mitrovica, J.X., Perron, J.T., Milne, G.A., Creveling, J.R., 2013. On postglacial sea level – III. Incorporating sediment redistribution. Geophys. J. Int. 194, 45–60. http://dx.doi.org/10.1093/gji/ggt089.
De Boer, B., Stocchi, P., Van de Wal, R.S.W., 2014. A fully coupled 3-D ice-sheet–sea-level model: algorithm and applications. Geosci. Model Dev. 7, 2141–2156.
De Boer, B., Wal, R.S.W., Lourens, L.J., Bintanja, R., Reerink, T.J., 2013. A continuous simulation of global ice volume over the past 1 million years with 3-D ice-sheet models. Clim. Dyn. 41, 1365–1384. http://dx.doi.org/10.1007/s00382-012-1562-2.
Deblonde, G., Peltier, W., Hyde, W., 1992. Simulations of continental ice sheet growth over the last glacial-interglacial cycle: experiments with a one level seasonal energy balance model including seasonal ice albedo feedback. Glob. Planet. Change 6, 37–55.
DeConto, R.M., Pollard, D., 2003. A coupled climate-ice sheet modeling approach to the early Cenozoic history of the Antarctic ice sheet. Palaeogeogr. Palaeoclimatol. Palaeoecol. 198, 39–42.
Depoorter, M.A., Bamber, J.L., Griggs, J.A., Lenaerts, J.T.M., Ligtenberg, S.R.M., van den Broeke, M.R., Moholdt, G., 2013. Calving fluxes and basal melt rates of Antarctic ice shelves. Nature 502, 89–93. http://dx.doi.org/10.1038/nature12567.
Dutton, A., Carlson, A.E., Long, A.J., Milne, G.A., Clark, P.U., DeConto, R., Horton, B.P., Rahmstorf, S., Raymo, M.E., 2015. Sea-level rise due to polar ice-sheet mass loss during past warm periods. Science 349.
Dziewonski, A.M., Anderson, D.I., 1981. Preliminary reference earth model (PREM). Phys. Earth Planet. Int. 25, 297–356.
Ehlers, J., Gibbard, P.L., 2007. The extent and chronology of Cenozoic global glaciation. Quat. Int. 164–165, 6–20.
Farrell, W.E., Clark, J.A., 1976. On postglacial sea level. Geophys. J. R. Astron. Soc. 46, 647–667.
Feldmann, J., Albrecht, T., Khroulev, C., Pattyn, F., Levermann, A., 2014. Resolution-dependent performance of grounding line motion in a shallow model compared with a full-stokes model according to the MISMIP3d intercomparison. J. Glaciol. 60, 353–360.
Fitzgerald, P.W., Bamber, J.L., Ridley, J.K., Rougier, J.C., 2012. Exploration of parametric uncertainty in a surface mass balance model applied to the Greenland ice sheet. J. Geophys. Res. 117 http://dx.doi.org/10.1029/2011JF002067.
Fretwell, P., Pritchard, H.D., Vaughan, D.G., Bamber, J.L., Barrand, N.E., Bell, R., Bianchi, C., Bingham, R.G., Blankenship, D.D., Casassa, G., Catania, G., Callens, D., Conway, H., Cook, A.J., Corr, H.F.J., Damaske, D., Damm, V., Ferraccioli, F., Forsberg, R., Fujita, S., Gim, Y., Gogineni, P., Griggs, J.A., Hindmarsh, R.C.A., Holmlund, P., Holt, J.W., Jacobel, R.W., Jenkins, A., Jokat, W., Jordan, T., King, E.C., Kohler, J., Krabill, W., Riger-Kusk, M., Langley, K.A., Leitchenkov, G., Leuschen, C., Luyendyk, B.P., Matsuoka, K., Mouginot, J., Nitsche, F.O., Nogi, Y., Nost, O.A., Popov, S.V., Rignot, E., Rippin, D.M., Rivera, A., Roberts, J., Ross, N., Siegert, M.J., Smith, A.M., Steinhage, D., Studinger, M., Sun, B., Tinto, B.K., Welch, B.C., Wilson, D., Young, D.A., Xiangbin, C., Zirizzotti, A., 2013. Bedmap2: improved ice bed, surface and thickness datasets for Antarctica. Cryosphere 7, 375–393.
Gladstone, R.M., Payne, A.J., Cornford, S.L., 2010. Parameterising the grounding line in flow-line ice sheet models. Cryosphere 4, 605–619. http://dx.doi.org/10.5194/tc-4-605-2010.
Golledge, N.R., Levy, R.H., McKay, R.M., Fogwill, C.J., White, D.A., Graham, A.G.C., Smith, J.A., Hillenbrand, C.D., Licht, K.J., Denton, G.H., Ackert Jr., R.P., Maas, S.M., Hall, B.L., 2013. Glaciology and geological signature of the Last Glacial Maximum antarctic ice sheet. Quat. Sci. Rev. 78, 225–247. http://dx.doi.org/10.1016/j.quascirev.2013.08.011.
Gomez, N., Mitrovica, J.X., Huybers, P., Clark, P.U., 2010. Sea level as a stabilizing factor for marine-ice-sheet grounding lines. Nat. Geosci. 3, 850–853.
Gomez, N., Pollard, D., Holland, D., 2015. Sea-level feedback lowers projections of future Antarctic ice-sheet mass loss. Nat. Commun. 6, 8798. http://dx.doi.org/10.1038/ncomms9798.
Gomez, N., Pollard, D., Mitrovica, J.X., 2013. A 3-D coupled ice sheet –sea level model applied to Antarctica through the last 40 ky. Earth Planet. Sci. Lett. 384, 88–99.
Gomez, N., Pollard, D., Mitrovica, J.X., Huybers, P., Clark, P.U., 2012. Evolution of a coupled marine ice sheet-sea level model. J. Geophys. Res. 117.
Grant, K.M., Rohling, E.J., Bar-Matthews, M., Ayalon, A., Medina-Elizalde, M., Ramsey, C.B., Satow, C., Roberts, A.P., 2012. Rapid coupling between ice volume and polar temperature over the past 150,000 years. Nature 491, 744–747. http://dx.doi.org/10.1038/nature11593.
Gudmundsson, G.H., Krug, J., Durand, G., Favier, L., Gagliardini, O., 2012. The stability of grounding lines on retrograde slopes. Cryosphere 6, 1497–1505. http://dx.doi.org/10.5194/tc-6-1497-2012.
Hansen, S.E., Graw, J.H., Kenyon, L.M., Nyblade, A.A., Wiens, D.A., Aster, R.C., Huerta, A.D., Anandakrishnan, S., Wilson, T., 2014. Imaging the Antarctic mantle using adaptively parameterized P-wave tomography: evidence for heterogeneous structure beneath West Antarctica. Earth Planet. Sci. Lett. 408, 66–78. http://dx.doi.org/10.1016/j.epsl.2014.09.043.
Heeszel, D.S., Wiens, D.A., Anandakrishnan, S., Aster, R.C., Dalziel, I.W.D., Huerta, A.D., Nyblade, A.A., Wilson, T.J., Winberry, J.P., 2016. Upper mantle structure of central and West Antarctica from array analysis of Rayleigh wave phase velocities. J. Geophys. Res. Solid Earth 121, 1758–1775. http://dx.doi.org/10.1002/2015JB012616.
Hughes, A.L.C., Gyllencreutz, R., Lohne, Ø.S., Mangerud, J., Svendsen, J.I., 2016. The last Eurasian ice sheets – a chronological database and time-slice reconstruction, DATED-1. Boreas 45, 1–45.
Hutter, L., 1983. Theoretical Glaciology. D. Reidel, Dordrecht.
Huybrechts, P., 1990. A 3-D model for the Antarctic ice sheet: a sensitivity study on the glacial-interglacial contrast. Clim. Dyn. 5, 79–92.
Huybrechts, P., 2002. Sea-level changes at the LGM from ice-dynamic reconstructions of the Greenland and Antarctic ice sheets during the glacial cycles. Quat. Sci. Rev. 21, 203–231.
Ingólfsson, Ó., Landvik, J.Y., 2013. The svalbard–barents sea ice-sheet –historical, current and future perspectives. Quat. Sci. Rev. 64, 33–60. http://dx.doi.org/10.1016/j.quascirev.2012.11.034.
Ivins, E.R., James, T.S., 2005. Antarctic glacial isostatic adjustment: a new assessment. Antarct. Sci. 17, 541–553.
Ivins, E.R., James, T.S., Wahr, J., O. Schrama, E.J., Landerer, F.W., Simon, K.M., 2013. Antarctic contribution to sea level rise observed by GRACE with improved GIA correction. J. Geophys. Res. Solid Earth 118, 3126–3141. http://dx.doi.org/10.1002/jgrb.50208.
Jamieson, S.S.R., Vieli, A., Livingstone, S.J., Cofaigh, C.O., Stokes, C., Hillenbrand, C.D., Dowdeswell, J.A., 2012. Ice-stream stability on a reverse bed slope. Nat. Geosci. 5, 799–802.
Johnston, P., 1993. The effect of spatially non-uniform water loads on predictions of sea level change. Geophys. J. Int. 114, 615–634.
Joughin, I., Alley, R.B., 2011. Stability of the West Antarctic ice sheet in a warming world. Nat. Geosci. 4, 506–513.
Jouzel, J., Masson-Delmotte, V., Cattani, O., Dreyfus, G., Falourd, S., Hoffmann, G., Minster, B., Nouet, J., Barnola, J.M., Chappellaz, J., Fischer, H., Gallet, J.C., Johnsen, S., Leuenberger, M., Loulergue, L., Luethi, D., Oerter, H., Parrenin, F., Raisbeck, G., Raynaud, D., Schilt, A., Schwander, J., Selmo, E., Souchez, R., Spahni, R., Stauffer, B., Steffensen, J.P., Stenni, B., Stocker, T.F., Tison, J.L., Werner, M., Wolff, E.W., 2007. Orbital and millennial Antarctic climate variability over the past 800,000 years. Science 317, 793–796.
Kendall, R., Latychev, K., Mitrovica, J., Davis, J., Tamisiea, M., 2006. Decontaminating tide gauge records for the influence of glacial isostatic adjustment: the potential

impact of 3-D Earth structure. Geophys. Res. Lett. 33 http://dx.doi.org/10.1029/2006GL028448.
Kendall, R.A., Mitrovica, J.X., Milne, G.A., 2005. On post-glacial sea level – II. Numerical formulation and comparative results on spherically symmetric models. Geophys. J. Int. 161, 679–706.
Kleman, J., Fastook, J., Ebert, K., Nilsson, J., Caballero, R., 2013. Pre-LGM Northern hemisphere ice sheet topography. Clim. Past 9, 2365–2378.
Konrad, H., Sasgen, I., Pollard, D., Klemann, V., 2015. Potential of the solid-earth response for limiting long-term West Antarctic Ice Sheet retreat in a warming climate. Earth Planet. Sci. Lett. 432, 254–264.
Konrad, H., Thoma, M., Sasgen, I., Klemann, V., Grosfeld, K., Barbi, D., Martinec, Z., 2014. The deformational response of a viscoelastic solid earth model coupled to a thermomechanical ice sheet model. Surv. Geophys. 35, 1441–1458. http://dx.doi.org/10.1007/s10712-013-9257-8.
Kopp, R.E., Simons, F.J., Mitrovica, J.X., Maloof, A.C., Oppenheimer, M., 2009. Probabilistic assessment of sea level during the last interglacial stage. Nature 462, 863–867.
Lambeck, K., Purcell, A., Funder, S., Kjaer, K.H., Larsen, E., Moller, P., 2006. Constraints on the late Saalian to early Middle Weichselian ice sheet of Eurasia from field data and rebound modelling. Boreas 35, 539–575. http://dx.doi.org/10.1080/03009480600781875.
Lambeck, K., Rouby, H., Purcell, A., Sun, Y., Sambridge, M., 2014. Sea level and global ice volumes from the Last Glacial Maximum to the holocene. Proc. Natl. Acad. Sci. 111, 15296–15303. http://dx.doi.org/10.1073/pnas.1411762111.
Lambeck, K., Smither, C., Ekman, M., 1998. Tests of glacial rebound models for Fennoscandinavia based on instrumented sea- and lake-level records. Geophys. J. Int. 135, 375–387.
Langebroek, P., Nisancioglu, K.H., 2014. Simulating last interglacial climate with NorESM: role of insolation and greenhouse gases in the timing of peak warmth. Clim. Past 10, 1305–1318. http://dx.doi.org/10.5194/cp-10-1305-2014.
Larour, E., Seroussi, H., Morlighem, M., Rignot, E., 2012. Continental scale, high order, high spatial resolution, ice sheet modeling using the Ice Sheet System Model (ISSM). J. Geophys. Res. Earth Surf. 117.
Laskar, J., Robutel, P., Joutel, F., Gastineau, M., Correia, A., Levrard, B., 2004. A long-term numerical solution for the insolation quantities of the Earth. Astron. Astroph 428, 261–285.
Latychev, K., Mitrovica, J., Tamisiea, M., Tromp, J., Christara, C., Moucha, R., 2005. Gia-induced secular variations in the Earth's long wavelength gravity field: influence of 3-D viscosity variations. Earth Planet. Sci. Lett. 240, 322–327. http://dx.doi.org/10.1016/j.epsl.2005.10.001.
Lecavalier, B.S., Milne, G.A., Simpson, M.J.R., Wake, L., Huybrechts, P., Tarasov, L., Kjeldsen, K.K., Funder, S., Long, A.J., Woodroffe, S., Dyke, A.S., Larsen, N.K., 2014. A model of Greenland ice sheet deglaciation constrained by observations of relative sea level and ice extent. Quat. Sci. Rev. 102, 54–84. http://dx.doi.org/10.1016/j.quascirev.2014.07.018.
Lisiecki, L., Raymo, M., 2005. A Pliocene-Pleistocene stack of 57 globally distributed benthic δ^{18} O records. Paleoceanography 20. http://dx.doi.org/10.1029/2004PA001071. PA1003.
Long, A., Barlow, N., Busschers, F., Cohen, K., Gehrels, W., Wake, L., 2015. Near-field sea-level variability in northwest Europe and ice sheet stability during the last interglacial. Quat. Sci. Rev. 126, 26–40. http://dx.doi.org/10.1016/j.quascirev.2015.08.021.
Maris, M.N.A., de Boer, B., Ligtenberg, S.R.M., Crucifix, M., van de Berg, W.J., Oerlemans, J., 2014. Modelling the evolution of the Antarctic ice sheet since the last interglacial. Cryosphere 8, 1347–1360. http://dx.doi.org/10.5194/tc-8-1347-2014.
Milne, Glenn, A., Mitrovica, Jerry, X., 1998. Postglacial sea-level change on a rotating Earth. Geophys. J. Int. 133, 1–19.
Milne, G., Mitrovica, J., 1996. Postglacial sea-level change on a rotating Earth: first results from a gravitationally self consistent sea-level equation. Geophys. J. Int. 126, F13–F20. http://dx.doi.org/10.1111/j.1365-246X.1996.tb04691.x.
Milne, G.A., Mitrovica, J.X., Davis, J.L., 1999. Near-field hydro-isostasy: the implementation of a revised sea-level equation. Geophys. J. Int. 139, 464–482. http://dx.doi.org/10.1046/j.1365-246x.1999.00971.x.
Mitrovica, J., Milne, G., 2003. On post-glacial sea level: I. General theory. Geophys. J. Int. 154, 253–267.
Mitrovica, J.X., Davis, J.L., Shapiro, I.I., 1994. A spectral formalism for computing three-dimensional deformations due to surface loads: 1. Theory. J. Geophys. Res. Solid Earth 99, 7057–7073. http://dx.doi.org/10.1029/93JB03128.
Mitrovica, J.X., Peltier, W.R., 1991. On post–glacial geoid subsidence over the equatorial ocean. J. Geophys. Res. 96, 20053–20071.
Morelli, A., Danesi, S., 2004. Seismological imaging of the Antarctic continental lithosphere: a review. Glob. Planet. Change 42, 155–165. http://dx.doi.org/10.1016/j.gloplacha.2003.12.005.
Morland, L.W., 1987. Unconfined ice-shelf flow. In: de Veen, C.J.V., Oerlemans, J. (Eds.), Dynamics of the West Antarctic Ice Sheet. D. Reidel, pp. 99–116.
NGRIP members, 2004. High-resolution record of Northern Hemisphere climate extending into the last interglacial period. Nature 431, 147–151.
Nield, G.A., Barletta, V.R., Bordoni, A., King, M.A., Whitehouse, P.L., Clarke, P.J., Domack, E., Scambos, T.A., Berthier, E., 2014. Rapid bedrock uplift in the Antarctic Peninsula explained by viscoelastic response to recent ice unloading. Earth Planet. Sci. Lett. 397, 32–41. http://dx.doi.org/10.1016/j.epsl.2014.04.019.
Nield, G.A., Whitehouse, P.L., King, M.A., Clarke, P.J., Bentley, M.J., 2012. Increased ice loading in the Antarctic Peninsula since the 1850s and its effect on glacial isostatic adjustment. Geophys. Res. Lett. 39, l17504. http://dx.doi.org/10.1029/2012GL052559.
Oerlemans, J., 1982. Glacial cycles and ice-sheet modelling. Clim. Change 4, 343–374.
O'Leary, M.J., Hearty, P.J., Thompson, W.G., Raymo, M.E., Mitrovica, J.X., Webster, J.M., 2013. Ice sheet collapse following a prolonged period of stable sea level during the last interglacial. Nat. Geosci. 6, 796–800. http://dx.doi.org/10.1038/ngeo1890.
Pattyn, F., Durand, G., 2013. Why marine ice sheet model predictions may diverge in estimating future sea level rise. Geophys. Res. Lett. 40, 4316–4320.
Pattyn, F., Perichon, L., Durand, G., Favier, L., Gagliardini, O., Hindmarsh, R.C., Zwinger, T., Albrecht, T., Cornford, S., Docquier, D., Fürst, J.J., Goldberg, D., Gudmundsson, G.H., Humbert, A., Hütten, M., Huybrechts, P., Jouvet, G., Kleiner, T., Larour, E., Martin, D., Morlighem, M., Payne, A.J., Pollard, D., Rückamp, M., Rybak, O., Seroussi, H., Thoma, M., Wilkens, N., 2013. Grounding-line migration in plan-view marine ice-sheet models: results of the ice2sea MISMIP3d intercomparison. J. Glaciol. 59, 410–422.
Pattyn, F., Schoof, C., Perichon, L., Hindmarsh, R.C.A., Bueler, E., de Fleurian, B., Durand, G., Gagliardini, O., Gladstone, R., Goldberg, D., Gudmundsson, G.H., Huybrechts, P., Lee, V., Nick, F.M., Payne, A.J., Pollard, D., Rybak, O., Saito, F., Vieli, A., 2012. Results of the marine ice sheet model intercomparison project, MISMIP. Cryosphere 6, 573–588. http://dx.doi.org/10.5194/tc-6-573-2012.
Peltier, W., Andrews, J., 1976. Glacial-Isostatic Adjustment-I. The forward problem. Geophys. J. R. Astron. Soc. 46, 605–646.
Peltier, W.R., 1974. The impulse response of a Maxwell Earth. Rev. Geophys. Space Phys. 12, 649–669.
Peltier, W.R., 1994. Ice age paleotopography. Science 265, 195–201.
Peltier, W.R., 1998. "implicit ice" in the global theory of glacial isostatic adjustment. Geophys. Res. Lett. 25, 3955–3958. http://dx.doi.org/10.1029/1998GL900076.
Peltier, W.R., 2004. Global glacial isostasy and the surface of the ice-age Earth: the ICE-5G (VM2) model and GRACE. Annu. Rev. Earth Planet Sci. 32, 111–149.
Peltier, W.R., Argus, D.F., Drummond, R., 2015. Space geodesy constrains ice age terminal deglaciation: the global ICE-6G_C (VM5a) model. J. Geophys. Res. Solid Earth 120, 450–487. http://dx.doi.org/10.1002/2014JB011176. 2014JB011176.
Peltier, W.R., Fairbanks, R.G., 2006. Global glacial ice volume and Last Glacial Maximum duration from an extended Barbados sea level record. Quat. Sci. Rev. 25, 3322–3337.
Petit, J.R., Jouzel, J., Raynaud, D., Barkov, N.I., Barnola, J.M., Basile, I., Bender, M., Chappellaz, J., Davis, M., Delaygue, G., Delmotte, M., Kotlyakov, V.M., Legrand, M., Lipenkov, V.Y., Lorius, C., PEpin, L., Ritz, C., Saltzman, E., Stievenard, M., 1999. Climate and atmospheric history of the past 420,000 years from the Vostok ice core, Antarctica. Nature 399, 429–436.
Philippon, G., Ramstein, G., Charbit, S., Kageyama, M., Ritz, C., Dumas, C., 2006. Evolution of the Antarctic ice sheet throughout the last deglaciation: a study with a new coupled climate–north and south hemisphere ice sheet model. Earth Planet. Sci. Lett. 248, 750–758.
Pollard, D., 1982. A simple ice sheet model yields realistic 100 kyr glacial cycles. Nature 296, 334–338.
Pollard, D., Chang, W., Haran, M., Applegate, P., DeConto, R., 2016. Large ensemble modeling of the last deglacial retreat of the West Antarctic Ice Sheet: comparison of simple and advanced statistical techniques. Geosci. Model Dev. 9, 1697–1723. http://dx.doi.org/10.5194/gmd-9-1697-2016.
Pollard, D., DeConto, R.M., 2009. Modelling West Antarctic ice sheet growth and collapse through the past five million years. Nature 458, 329–332.
Pollard, D., DeConto, R.M., 2012. Description of a hybrid ice sheet-shelf model, and application to Antarctica. Geosci. Model Dev. 5, 1273–1295.
Pollard, D., DeConto, R.M., Alley, R.B., 2015. Potential Antarctic Ice Sheet retreat driven by hydrofracturing and ice cliff failure. Earth Planet. Sci. Lett. 412, 112–121.
Rignot, E., Mouginot, J., Scheuchl, B., 2011. Ice flow of the Antarctic ice sheet. Science 333, 1427–1430.
Ritz, C., Fabre, A., Letréguilly, A., 1997. Sensitivity of a Greenland ice sheet model to ice flow and ablation parameters: consequences for the evolution through the last climatic cycle. Clim. Dyn. 13, 11–24.
Robel, A.A., Schoof, C., Tziperman, E., 2016. Persistence and variability of ice-stream grounding lines on retrograde bed slopes. Cryosphere 10, 1883–1896. http://dx.doi.org/10.5194/tc-10-1883-2016.
Rohling, E.J., Grant, K., Hemleben, C., Siddall, M., Hoogakker, B.A.A., Bolshaw, M., Kucera, M., 2008. High rates of sea-level rise during the last interglacial period. Nat. Geosci. 1, 38–42.
Rovere, A., Raymo, M.E., Vacchi, M., Lorscheid, T., Stocchi, P., Gómez-Pujol, L., Harris, D.L., Casella, E., O'Leary, M.J., Hearty, P.J., 2016. The analysis of last interglacial (MIS 5e) relative sea-level indicators: reconstructing sea-level in a warmer world. Earth-Science Rev. 159, 404–427.
Schoof, C., 2007. Ice sheet grounding line dynamics: steady states, stability, and hysteresis. J. Geophys. Res. 112 http://dx.doi.org/10.1029/2006JF000664.
Seroussi, H., Morlighem, M., Larour, E., Rignot, E., Khazendar, A., 2014. Hydrostatic grounding line parameterization in ice sheet models. Cryosphere 8, 2075–2087. http://dx.doi.org/10.5194/tc-8-2075-2014.
Simon, K., James, T., Dyke, A., 2015. A new glacial isostatic adjustment model of the Innuitian Ice Sheet, Arctic Canada. Quat. Sci. Rev. 119, 11–21. http://dx.doi.org/10.1016/j.quascirev.2015.04.007.
Simpson, M.J., Milne, G.A., Huybrechts, P., Long, A.J., 2009. Calibrating a glaciological model of the Greenland ice sheet from the Last Glacial Maximum to present-day using field observations of relative sea level and ice extent. Quat. Sci. Rev. 28, 1631–1657. http://dx.doi.org/10.1016/j.quascirev.2009.03.004.

Spada, G., Antonioli, A., Boschi, L., Brandi, V., Cianetti, S., Galvani, G., Giunchi, C., Perniola, B., Piana Agostinetti, N., Piersanti, A., Stocchi, P., 2004. Modeling Earth's post-glacial rebound. EOS, Trans. Am. Geophys. Union 85, 62–64.
Spada, G., Stocchi, P., 2007. SELEN: a Fortran 90 program for solving the "sea-level equation". Comput. Geosci. 33, 538–562.
Stokes, C.R., Tarasov, L., Blomdin, R., Cronin, T.M., Fisher, T.G., Gyllencreutz, R., Hv§ttestrand, C., Heyman, J., Hindmarsh, R.C., Hughes, A.L., Jakobsson, M., Kirchner, N., Livingstone, S.J., Margold, M., Murton, J.B., Noormets, R., Peltier, W.R., Peteet, D.M., Piper, D.J., Preusser, F., Renssen, H., Roberts, D.H., Roche, D.M., Saint-Ange, F., Stroeven, A.P., Teller, J.T., 2015. On the reconstruction of palaeo-ice sheets: recent advances and future challenges. Quat. Sci. Rev. 125, 15–49. http://dx.doi.org/10.1016/j.quascirev.2015.07.016.
Stone, E.J., Lunt, D.J., Annan, J.D., Hargreaves, J.C., 2013. Quantification of the Greenland ice sheet contribution to Last Interglacial sea level rise. Clim. Past 9, 621–639. http://dx.doi.org/10.5194/cp-9-621-2013.
Stuhne, G.R., Peltier, W.R., 2015. Reconciling the ICE-6G_C reconstruction of glacial chronology with ice sheet dynamics: the cases of Greenland and Antarctica. J. Geophys. Res. Earth Surf. 120, 1841–1865.
Tarasov, L., Dyke, A.S., Neal, R.M., Peltier, W.R., 2012. A data-calibrated distribution of deglacial chronologies for the North American ice complex from glaciological modeling. Earth Planet. Sci. Lett. 315–316, 30–40.
Tarasov, L., Peltier, W., 2004. A geophysically constrained large ensemble analysis of the deglacial history of the North American ice-sheet complex. Quat. Sci. Rev. 23, 359–388. http://dx.doi.org/10.1016/j.quascirev.2003.08.004.
Tarasov, L., Peltier, W.R., 1999. Impact of thermomechanical ice sheet coupling on a model of the 100 kyr ice age cycle. J. Geophys. Res. Atmos. 104, 9517–9545.
Tarasov, L., Peltier, W.R., 2002. Greenland glacial history and local geodynamic consequences. Geophys. J. Int. 150, 198–229.
Tarasov, L., Peltier, W.R., 2003. Greenland glacial history, borehole constraints, and Eemian extent. J. Geophys. Res. 108 http://dx.doi.org/10.1029/2001JB001731.
Tegmark, M., 1996. An icosahedron-based method for pixelizing the celestial sphere. Astrophys. J. Lett. 470, L81–L84.
Thompson, W.G., Goldstein, S.L., 2005. Open-system coral ages reveal persistent suborbital sea-level cycles. Science 308, 401–404. http://dx.doi.org/10.1126/science.1104035.
Tushingham, A.M., Peltier, W.R., 1992. Validation of the ICE-3G model of Würm-Wisconsin deglaciation using a global data base of relative sea level histories. J. Geophys. Res. 97, 3285–3304.
Vermeersen, L., Sabadini, R., 1999. Polar wander, sea-level variations and ice age cycles. Surv. Geophys. 20, 415–440.
Van de Wal, R.S.W., 1999. Processes of buildup and retreat of the Greenland ice sheet. J. Geophys. Res. 104, 3899–3906. http://dx.doi.org/10.1029/1998JD200030.
Van der Wal, W., Barnhoorn, A., Stocchi, P., Gradmann, S., Wu, P., Drury, M., Vermeersen, B., 2013. Glacial isostatic adjustment model with composite 3-D Earth rheology for Fennoscandia. Geophys. J. Int. 194, 61–77. http://dx.doi.org/10.1093/gji/ggt099.
Van der Wal, W., Whitehouse, P.L., Schrama, E.J., 2015. Effect of GIA models with 3D composite mantle viscosity on GRACE mass balance estimates for Antarctica. Earth Planet. Sci. Lett. 414, 134–143. http://dx.doi.org/10.1016/j.epsl.2015.01.001.
Weertman, J., 1974. Stability of the junction of an ice sheet and an ice shelf. J. Glaciol. 13, 3–11.
Whitehouse, P., Latychev, K., Milne, G., Mitrovica, J., Kendall, R., 2006. Impact of 3-D Earth structure on Fennoscandian glacial isostatic adjustment: implications for space-geodetic estimates of present-day crustal deformations. Geophys. Res. Lett. 33 http://dx.doi.org/10.1029/2006GL026568.
Whitehouse, P.L., Bentley, M.J., Le Brocq, A.M., 2012a. A deglacial model for Antarctica: geological constraints and glaciological modelling as a basis for a new model of antarctic glacial isostatic adjustment. Quat. Sci. Rev. 32, 1–24.
Whitehouse, P.L., Bentley, M.J., Milne, G.A., King, M.A., Thomas, I.D., 2012b. A new glacial isostatic adjustment model for Antarctica: calibrated and tested using observations of relative sea-level change and present-day uplift rates. Geophys. J. Int. 190, 1464–1482.
Woodward, R., 1888. On the form and position of mean sea level. U. S. Geol. Surv. Bull. 48, 87–170.
Wu, P., Peltier, W., 1984. Pleistocene deglaciation and the Earth's rotation: a new analysis. Geophys. J. R. Astron. Soc. 76, 753–791.
Zweck, C., Huybrechts, P., 2005. Modeling of the northern hemisphere ice sheets during the last glacial cycle and glaciological sensitivity. J. Geophys. Res. 110.